Journal of Magnetic Resonance 210 (2011) 246–259

Contents lists available at ScienceDirect

Journal of Magnetic Resonance

journal homepage: www.elsevier.com/locate/jmr

Accurate measurement of one-bond H–X heteronuclear dipolar couplings in MAS solid-state NMR

Paul Schanda [a,b], Beat H. Meier [a], Matthias Ernst [a,*]

[a] Physical Chemistry, ETH Zürich, Wolfgang-Pauli-Strasse 10, 8093 Zürich, Switzerland
[b] Institut de Biologie Structurale Jean-Pierre Ebel, CNRS-CEA, Univ. Grenoble 1, 41, rue Jules Horowitz, F-38027 Grenoble Cedex, France

ARTICLE INFO

Article history:
Received 7 January 2011
Revised 8 March 2011
Available online 21 March 2011

Keywords:
Solid-state NMR
REDOR
Order parameter
Dynamic measurement

ABSTRACT

The accurate experimental determination of dipolar-coupling constants for one-bond heteronuclear dipolar couplings in solids is a key for the quantification of the amplitudes of motional processes. Averaging of the dipolar coupling reports on motions on time scales up to the inverse of the coupling constant, in our case tens of microseconds. Combining dipolar-coupling derived order parameters that characterize the amplitudes of the motion with relaxation data leads to a more precise characterization of the dynamical parameters and helps to disentangle the amplitudes and the time scales of the motional processes, which impact relaxation rates in a highly correlated way. Here. we describe and characterize an improved experimental protocol – based on REDOR – to measure these couplings in perdeuterated proteins with a reduced sensitivity to experimental missettings. Because such effects are presently the dominant source of systematic errors in experimental dipolar-coupling measurements, these compensated experiments should help to significantly improve the precision of such data. A detailed comparison with other commonly used pulse sequences (T-MREV, phase-inverted CP, $R18_2^5$, and $R18_1^7$) is provided.

1. Introduction

Accurate measurements of one-bond dipolar couplings in solid-state NMR are of great interest in the context of characterizing backbone and side-chain dynamics in biological molecules [1–9]. The partial averaging of dipolar couplings gives information about the amplitude of the motional processes from the fastest time scales up to the time scale corresponding to the inverse of the coupling strength, i.e., typically up to tens of microseconds. In the case of isotropic motions, the amplitude is often expressed in terms of an order parameter S which simply expresses the ratio of the measured dipolar-coupling anisotropy and the theoretical rigid-limit value and, therefore, characterizes the scaling of the dipolar coupling. Obviously, no information about the actual time scales can be obtained from such measurements. Information about the time scales is available from relaxation data that can be used to supplement the information obtained from dipolar-coupling measurements [6,7,9,10]. In principle, relaxation data measured at different B_0-field strengths allow a separation of time scales and motional amplitudes but due to the weak dependence of the relaxation-rate constants on the magnetic field strength such a determination is often not very precise for experimental data sets [10,11]. Dipolar couplings are, thus, a very useful complement to relaxation data, and are generally required if motional amplitudes and time scales are to be analyzed quantitatively.

Heteronuclear dipolar couplings can generally be measured under magic-angle spinning (MAS) conditions using recoupling sequences, where the evolution of an initial density operator prepared to be proportional to S_x is observed during a recoupling sequence. Preparation of this initial in-phase S_x magnetization can be achieved by cross polarization from protons using the dipolar coupling or by an INEPT-type pulse scheme, based on the scalar coupling. The general scheme for the latter approach of measuring one-bond dipolar couplings is shown in Fig. 1 which uses two refocused INEPT blocks [12,13] for polarization transfer from the I spins to the S spins and back. Such an INEPT-transfer based approach is best suited for isotopically diluted spin systems where most of the protons are replaced by deuterons because dephasing of transverse magnetization in such samples is slow enough to allow efficient heteronuclear polarization transfer. It is often possible to achieve either reprotonation of exchangeable proton sites by an appropriate choice of the solvent, selective protonation of methyls [14,15] or stochastic protonation of aliphatic sites [16]. Of course, other polarization-transfer method such as Hartmann–Hahn cross polarization [17] can also be used instead. The measurement of the dipolar couplings is implemented as a dephasing period after the t_1 time (see Fig. 1) where the heteronuclear dipolar coupling is recoupled by a suitable pulse sequence. Variations of this scheme and more elaborate pulse schemes are possible. Measuring a series of two-dimensional heteronuclear chemical-shift correlation spectra

* Corresponding author. Fax: +41 1 632 1621.
E-mail address: maer@ethz.ch (M. Ernst).

1090-7807/$ - see front matter © 2011 Elsevier Inc. All rights reserved.
doi:10.1016/j.jmr.2011.03.015

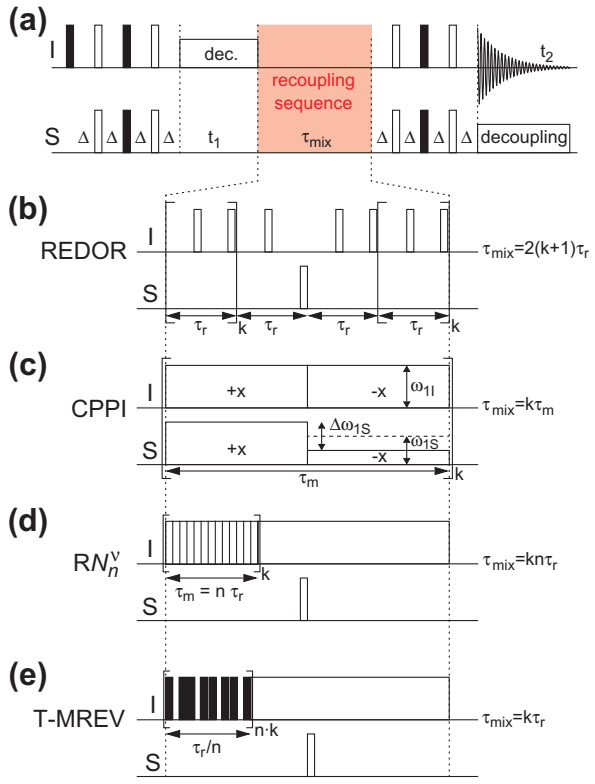

Fig. 1. Schematic drawing of the pulse sequences used for measuring heteronuclear dipolar couplings.

as a function of the dephasing time τ_{mix} allows the determination of the dipolar-coupling constants from the modulation of the cross-peak intensities. In principle, it is also possible to determine the dipolar couplings from the oscillation in a polarization-transfer experiment, such as in CP experiments, rather than from a dephasing experiment. One method that was used very early on is Lee–Goldburg cross polarization (LG CP) [18,19] where the abundant spins are spin locked along the magic angle to average out homonuclear dipolar couplings [20]. This method has been used to measure C–H dipolar couplings in uniformly ^{13}C- and ^{15}N-labeled ubiquitin [2–4] but it is well known that the averaging of the homonuclear dipolar couplings is incomplete in such experiments [21,22]. In addition, this approach suffers from rf-field miscalibration and inhomogeneities in the same manner as CP experiments [23]. We will focus here only on experiments that are based on a dephasing of in-phase S_x coherence.

Several methods have been proposed to measure the magnitude of one-bond dipolar couplings in proteins. One approach is the use of the transverse MREV (T-MREV) pulse sequence [24] which also leads to a partial averaging of the homonuclear dipolar coupling while the heteronuclear dipolar couplings are retained with a scaling factor. The T-MREV sequence has been used to measure N–H and C–H dipolar couplings in fully protonated GB1 [1] and N–H dipolar couplings in fully protonated huPrP23-144 [7]. Symmetry-based pulse sequences [25] can also be used to selectively reintroduce the heteronuclear dipolar coupling while at the same time suppressing the homonuclear dipolar coupling. The $R18_1^7$ sequence [26] has been used to measure N–H couplings in fully protonated thioredoxin [6] and the $R18_2^5$ sequence has been used to quantify N–H dipolar couplings in the context of hydrogen bonding [27].

Because perdeuteration of proteins (and reintroducing some protons) has been shown to have a number of advantages, most importantly a high resolution in the ^{1}H spectrum and the possibility for sensitive proton detection, experimental schemes for such proteins have also been developed. Here the design can concentrate more on the compensation of systematic errors introduced by non idealities in the experiment, because the suppression of the homonuclear dipolar interaction is not any more the dominant design requirement. A variation of the CP experiment, called phase-inverted CP (CPPI) [23,28] was used to measure N–H dipolar couplings in a highly-deuterated SH3 domain [5]. REDOR techniques [29–31] are another attractive choice in such systems. Using a shifted-time finite-pulse version of REDOR, N–H dipolar couplings in highly-deuterated ubiquitin have been measured [9]. There are also measurements of N-C dipolar couplings using the TEDOR [32] pulse sequence applied to fully protonated huPrP23-144 [7]. Multiple-quantum correlation spectroscopy [33,34] has also been used to measure C–C dipolar couplings [8].

The accuracy of the experimental measurement of dipolar couplings is crucial, especially if motional amplitudes in different proteins are to be compared, or if dipolar couplings are used in combination with relaxation data in order to describe time scales and amplitudes quantitatively. Therefore, we assess here the accuracy of different recoupling experiments by determining the magnitude of systematic errors that arise from miscalibrations of the radio-frequency amplitude, the influence of homonuclear dipolar couplings, chemical-shift offsets and CSA parameters, and the combined effect of miscalibrations of rf fields and homonuclear dipolar couplings. We decided to investigate five different pulse schemes, namely the CPPI scheme, the $R18_1^7$ and $R18_2^5$ pulse sequences, the T-MREV sequence and the REDOR scheme using numerical simulations.

This article is organized as follows: Section 2 provides a theoretical description of the different recoupling schemes. It is intended for the interested reader, but not an absolute necessity for the reader mainly interested in choosing and implementing a recoupling experiment for practical use. Section 3 investigates the robustness of the different pulse schemes using numerical simulations. From these numerical simulations we conclude that the REDOR scheme which can be used for a wide range of spinning frequencies gives the lowest systematic errors for samples with low proton density. For samples with dense proton coupling networks (as non-deuterated protein samples), the T-MREV sequence leads to accurate results for slow to intermediate MAS frequencies. In Section 4 we show experimental data of N–H dipolar-coupling measurements with a REDOR experiment, measured on a highly deuterated preparation of the protein ubiquitin.

2. Theory

2.1. REDOR experiments

For the analytical description of the REDOR experiment [29,30] we consider a heteronuclear dipolar-coupled two-spin system in a strong magnetic field with a rotating-frame Hamiltonian of

$$\mathscr{H}_{IS}(t) = 2I_zS_z\sum_{n=-2}^{2}\omega_{IS}^{(n)}e^{in\omega_r t} \tag{1}$$

with $\omega_{IS}^{(n)} = \frac{1}{2}\cdot d_{n,0}^2(-\theta_m)\cdot e^{-in\gamma}\cdot d_{0,n}^2(\beta)\cdot\delta_{IS}$. Here, β and γ are the Euler angles describing the orientation of a crystallite in the rotor-fixed frame, θ_m is the magic angle, and the $d_{n,n'}(\beta)$ are the reduced Wigner rotation-matrix elements [35]. The anisotropy parameter of the dipolar-coupling tensor is given by

$$\delta_{IS} = -2\frac{\mu_0}{4\pi}\frac{\gamma_I\gamma_S\hbar}{r_{IS}^3} \tag{2}$$

The timing of a standard REDOR experiment with finite pulses is shown in Fig. 2a with the pulse length given by $\tau_P = \frac{\phi}{2}\tau_r$ and $\omega_r/\omega_1 = \phi$. The first-order average Hamiltonian (often also termed

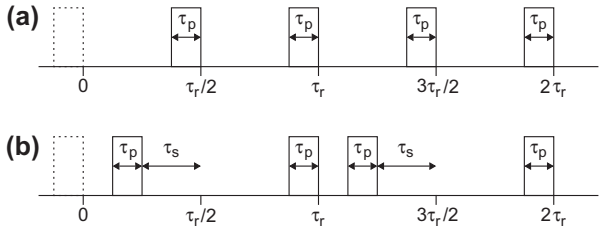

Fig. 2. Timing of (a) the standard REDOR pulse sequence and (b) the shifted REDOR pulse sequence. Shown is only the first half of the REDOR recoupling train, preceding the π pulse on the S spin. The sequence in (b) is applied in a mirror-symmetric manner in the second half [30].

the zeroth-order average Hamiltonian)[1] for standard finite-pulse REDOR experiment has been solved analytically [31] leading with an alternation of the phases of subsequent π pulses during the recoupling pulse train following the xy-4 scheme [40] to a Hamiltonian of the form

$$\mathscr{H}_{IS}^{(1)} = \frac{-\delta_{IS}}{\sqrt{2}\pi}\frac{\cos\left(\frac{\pi\phi}{2}\right)\sin(2\beta)\sin\left(\gamma-\frac{\pi\phi}{2}\right)}{1-\phi^2}2I_zS_z \tag{3}$$

In the limit of strong rf pulses $\phi \to 0$, we obtain the well known result for the REDOR experiment with δ pulses, namely

$$\overline{\mathscr{H}}_{IS}^{(1)} = \frac{-\delta_{IS}}{\sqrt{2}\pi}\sin(2\beta)\sin(\gamma)2I_zS_z \tag{4}$$

The finite pulses lead to a scaling of the REDOR oscillation frequency by

$$\kappa = \frac{\cos(\pi\phi/2)}{1-\phi^2} \tag{5}$$

We now consider a finite-pulse REDOR experiment where the pulses in the center of each rotor period (at $n\tau_r/2$) are shifted to the left by $\tau_s = \varepsilon\tau_r/2$ (see Fig. 2b) in the first half of the REDOR sequence and to the right in the second half of the REDOR sequence [30]. A calculation similar to the finite-pulse REDOR experiment [31] leads, with the phases following the xy-4 scheme, to a first-order average Hamiltonian of

$$\begin{aligned}\overline{\mathscr{H}}_{IS}^{(1)} = &\frac{\delta_{IS}}{4\pi(4\phi^4-5\phi^2+1)}\\ &\times\Big[(\phi^2-1)\sin^2(\pi\varepsilon)\cos(\pi\phi)\sin^2(\beta)\sin(2\gamma-\pi\phi)\\ &+2\sqrt{2}(4\phi^4-1)\cos^2\left(\frac{\pi\varepsilon}{2}\right)\cos\left(\frac{\pi\phi}{2}\right)\sin(2\beta)\sin\left(\gamma-\frac{\pi\phi}{2}\right)\Big]2I_zS_z\end{aligned} \tag{6}$$

This Hamiltonian contains contributions from the $\omega_{IS}^{(\pm1)}$ and $\omega_{IS}^{(\pm2)}$ component of the dipolar coupling while only $\omega_{IS}^{(\pm1)}$ contributes in the standard REDOR experiment. In the limiting case of $\varepsilon \to 0$ we obtain back the average Hamiltonian of Eq. (3) while in the limit of $\varepsilon \to 1$ we obtain $\overline{\mathscr{H}}_{IS}^{(1)} = 0$. The Hamiltonian of the shifted finite-pulse REDOR experiment contains a scaled effective dipolar coupling with a scaling factor that can be adjusted by the experimentalist through the choice of the pulse timing. Note, that the scaling factor depends on the crystallite orientation and is not uniform over a powder sample. In the limit of δ pulses ($\phi \to 0$), Eq. (6) reduces to the well-known expression [30]

$$\begin{aligned}\overline{\mathscr{H}}_{IS}^{(1)} = &\frac{-\delta_{IS}}{4\pi}\Big[\sin^2(\pi\varepsilon)\sin^2\beta\sin(2\gamma)\\ &+2\sqrt{2}\cos^2\left(\frac{\pi\varepsilon}{2}\right)\sin(2\beta)\sin\gamma\Big]2I_zS_z\end{aligned} \tag{7}$$

A more general solution for an asymmetric-dipolar coupling tensor can be found in the Supporting Information.

Given the fact, that the time evolution under the REDOR sequence can only be sampled at integer multiples of the cycle time $\tau_c = 2\tau_r$, such a scaling is a useful property that can be used to obtain a better experimental sampling of the REDOR curve for large dipolar couplings. This is an important feature for the measurement of one-bond N–H or C–H couplings which are of the order of 23 and 43 kHz, respectively. The scaling of the REDOR recoupling is illustrated in Fig. 3 where the maximum dipolar splitting (i.e. the maximum value of the prefactor in front of the $2I_zS_z$ term in Eq. (6) over the powder distribution) is shown as a function of the position of the shifted pulse (expressed in ε) for four different ratios of spinning frequency to rf amplitude $\omega_r/\omega_1 = \phi$ (Fig. 3a). As predicted, the width of the powder pattern is reduced with increasing values

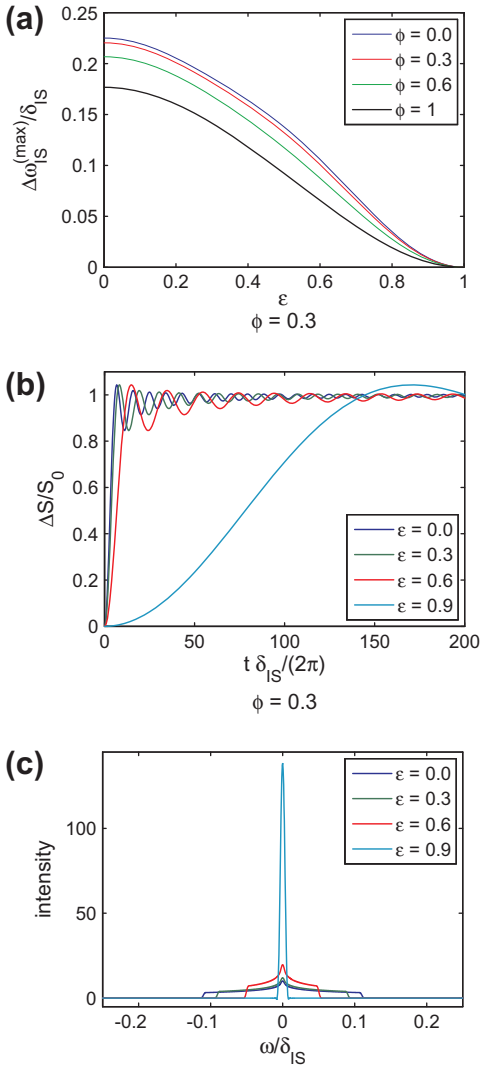

Fig. 3. Analytical calculation of REDOR characteristics and REDOR curves as a function of the parameters $\phi = \omega_r/\omega_1$ and $\varepsilon = 2\tau_s/\tau_r$. (a) Plot of the maximum dipolar splitting $\Delta\omega_{IS}^{(maz)}/\delta_{IS}$ as a function of ε for three different values of ϕ. The curve for $\phi = 0$ represents the δ-pulse limit. (b) REDOR curves $\Delta S/S_0$ plotted as a function of $t\delta_{IS}/(2\pi)$ for $\phi = 0.3$ and values of $\varepsilon = 0$, 0.3, 0.6, and 0.9. (c) Powder patterns corresponding to the four REDOR dephasing curves in (b).

[1] In the past we have used a numbering of the average Hamiltonian starting from 0 as it was introduced by Haeberlen and Waugh [36,37]. Such a numbering leads to differences between AHT and Floquet treatments [38] where comparable terms appear in the Floquet treatment in order (n) while they appear in order ($n-1$) in the AHT expansion. We have, therefore, decided to follow the convention suggested by Hohwy et al. [39] and start the numbering of the AHT expansion with 1.

of ε. This can also be seen from a plot of the REDOR curves in Fig. 3b where the REDOR oscillations become slower and the corresponding powder patterns (Fig. 3c) narrower with increasing value of ε. The differences between the curves for different values of $\omega_r/\omega_1 = \phi$ are small (Fig. 3a) showing that the xy-4 scheme partially eliminates the effects of finite pulses [31]. Since each rotor period contains two 180° pulses, the rf-field requirement for the finite-pulse REDOR experiment is $\omega_1 \geqslant \omega_r$ (see Fig. 2) which makes it a quite suitable experiment for fast MAS.

While homonuclear dipolar couplings vanish in the hard pulse limit, they are partially recoupled in the finite-pulse REDOR experiment. Analytical expressions for the first-order average Hamiltonian under the shifted finite-pulse REDOR experiment can be found in Eq. (S5) of the Supplementary Information. With increasing field strength, i.e., smaller values of ϕ, the magnitude of the first-order average Hamiltonian decreases. Therefore, it is advisable to use high rf fields in order to minimize the recoupling of homonuclear dipolar couplings.

The dephasing in the REDOR experiment is simple and evolves according to a powder average over cosine functions, $\cos(\omega t)$, where ω denotes the entire prefactor in front of the $2I_zS_z$ spin-operator term in the first-order average Hamiltonian of the REDOR pulse sequence (Eqs. (3), (6), or (7)). The REDOR experiment has the added benefit (over the other pulse sequences shown in Fig. 1) that a control experiment without recoupling can be implemented by leaving out the refocusing pulses on the I spins (Fig. 1c). This control experiment compensates the signal loss of the magnetization due to relaxation. Therefore, the REDOR curve $\Delta S/S_0$ can be fitted with a single free parameter, the dipolar coupling δ_{IS}. Furthermore, the REDOR pulse sequence is the only sequence of the ones considered here that produces, to first-order average-Hamiltonian theory, an Ising-type Hamiltonian of the form $\sum_{i,j} 2I_{iz}S_{jz}$. In the case of more than 2 spins, this Hamiltonian is not susceptible to dipolar-truncation phenomena [33,41–43]. Note, that for the finite-pulse REDOR experiment the Hamiltonian has only such an Ising-type form if the xy-4 [40] scheme is used [31]. The xy-4 scheme is a prerequisite for the robustness of the experiment (see Fig. S1 in the Supplementary Material). Without the phase cycle, the Hamiltonian has two terms of the form $2I_zS_z$ and $2I_yS_z$ which do not commute and can lead to dipolar truncation effects.

2.2. Phase-inverted cross-polarization experiment

The phase-inverted cross-polarization (CPPI) [28,23] experiment uses a periodic inversion of the rf phase on both channels with a simultaneous change of the Hartmann–Hahn side-band matching condition under MAS from $n = +1$ to $n = -1$. This implies a change of the rf-field amplitude by $2\omega_r$ on one of the channels (Fig. 1c). Such an experiment can be viewed as a phase-alternating irradiation (XiX) on the I spins with amplitude ω_{1I} and on the S spins with amplitude ω_{1S} with a modulation frequency $\omega_m = 2\pi/\tau_m$. Superimposed on the phase-alternating irradiation, there is an additional cw irradiation on the S spins with amplitude $\Delta\omega_{1S}/2 = \omega_r$. Such an experiment can be described by operator-based Floquet theory [44] using three basic frequencies after an interaction-frame transformation that eliminates the rf-field part of the Hamiltonian

$$U(t) = \exp\left(-i\beta_I(t)\sum_\ell I_{\ell z}\right)\exp\left(-i\frac{\pi}{2}\sum_\ell I_{\ell y}\right) \times \exp\left(-i\beta_S(t)\sum_\ell S_{pz}\right)\exp\left(-i\frac{\Delta\omega_{1S}}{2}t\sum_p S_{pz}\right) \times \exp\left(-i\frac{\pi}{2}\sum_p S_{py}\right) \tag{8}$$

where the time-dependent flip angles $\beta_I(t)$ and $\beta_S(t)$ lead to an interaction-frame transformation of the form

$$\widetilde{I}_x(t) = I_x\cos(\beta_I(t)) + I_y\sin(\beta_I(t)) = \sum_{k=-\infty}^{\infty}\left(I_x a_{Ix}^{(k)} + I_y a_{Iy}^{(k)}\right)e^{ik\omega_m t} \tag{9}$$

and

$$\widetilde{S}_x(t) = S_x\cos(\beta_S(t)) + S_y\sin(\beta_S(t)) = \sum_{k=-\infty}^{\infty}\left(S_x a_{Sx}^{(k)} + S_y a_{Sy}^{(k)}\right)e^{ik\omega_m t} \tag{10}$$

respectively. The time-dependent interaction-frame Hamiltonian is given by

$$\mathscr{H}(t) = \sum_{n=-2}^{2}\sum_{k=-\infty}^{\infty}\sum_{\ell=-2}^{2}\mathscr{H}^{(n,k,\ell)}e^{in\omega_r t}e^{ik\omega_m t}e^{i\ell\frac{\Delta\omega_{1S}}{2}t} \tag{11}$$

Neglecting all isotropic J couplings and considering a Hamiltonian that contains only isotropic chemical shifts, CSA tensors, and dipolar couplings leads to Fourier coefficients that are given by

$$\widetilde{\mathscr{H}}^{(0,0,0)} = \sum_d \omega_{I_d}^{(0)}\left(a_{Ix}^{(0)}I_{dx} + a_{Iy}^{(0)}I_{dy}\right)$$

$$\begin{aligned}\widetilde{\mathscr{H}}^{(n,0,0)} = &\sum_d \omega_{I_d}^{(n)}\left(a_{Ix}^{(0)}I_{dx} + a_{Iy}^{(0)}I_{dy}\right)\\ &-\sum_{d<e}\omega_{I_dI_e}^{(n)}\left[I_{dz}I_{ez} - \frac{1}{2}(I_{dx}I_{ex} + I_{dy}I_{ey})\right]\\ &-\sum_{p<q}\omega_{S_pS_q}^{(n)}\left[S_{pz}S_{qz} - \frac{1}{2}(S_{px}S_{qx} + S_{py}S_{qy})\right]\\ &-\sum_{d<e}\frac{3}{2}\omega_{I_dI_e}^{(n)}\left((I_{dx}I_{ex} + I_{dy}I_{ey})b_{Ix}^{(0)} + (I_{dx}I_{ey} + I_{dy}I_{ex})b_{Iy}^{(0)}\right)\end{aligned}$$

$$\begin{aligned}\widetilde{\mathscr{H}}^{(n,k,0)} = &\sum_d \omega_{I_d}^{(n)}\left(a_{Ix}^{(k)}I_{dx} + a_{Iy}^{(k)}I_{dy}\right)\\ &+\sum_{d<e}\frac{3}{2}\omega_{I_dI_e}^{(n)}\left((I_{dx}I_{ex} + I_{dy}I_{ey})b_{Ix}^{(k)} + (I_{dx}I_{ey} + I_{dy}I_{ex})b_{Iy}^{(k)}\right)\end{aligned}$$

$$\begin{aligned}\widetilde{\mathscr{H}}^{(n,k,\pm1)} = &\sum_{d,p}\omega_{S_pI_p}^{(n)}S_p^{\pm}\left(I_{dx}\left(b_{xx}^{(k)} \pm ib_{xy}^{(k)}\right) - I_{dy}\left(b_{yx}^{(k)} \pm ib_{yy}^{(k)}\right)\right)\\ &-\frac{1}{2}\sum_p\omega_{S_p}^{(n)}S_q^{\pm}\left(a_{Sx}^{(k)} \pm ib_{Sy}^{(k)}\right)\end{aligned}$$

$$\widetilde{\mathscr{H}}^{(n,k,\pm2)} = \sum_{p<q}\frac{3}{4}\omega_{S_pS_p}^{(n)}S_p^{\pm}S_q^{\pm}\left(b_{Sx}^{(k)} \pm ib_{Sy}^{(k)}\right) \tag{12}$$

where the $a_S^{(k)} = a_{Sx}^{(k)} + ia_{Sy}^{(k)}$ and the $b_S^{(k)} = b_{Sx}^{(k)} + ib_{Sy}^{(k)}$ are the Fourier coefficients of the $\exp(i\beta_S(t))$ and $\exp(2i\beta_S(t))$ terms, respectively, as defined by Eqs. (9) and (10). They can either be calculated numerically or analytically using an infinite sum over Bessel functions [45]. The amplitude of the rf field does not enter directly into the interaction-frame transformation but indirectly through the magnitude of the $a_S^{(k)}$ and $b_S^{(k)}$ coefficients. Typically, the $a_S^{(k)}$ coefficients are maximum for $k^{(\max)} = \omega_{1S}/\omega_m$ while the $b_S^{(k)}$ coefficients are maximum for $k^{(\max)} = 2\omega_{1S}/\omega_m$ [45]. The same expressions hold for the $a_I^{(k)}$ and $b_I^{(k)}$ coefficients. The $b_{\mu\nu}^{(k)}$ coefficients describe combined modulations by the irradiation on the I and S spins and are defined as

$$b_{\mu\nu}^{(k)} = \sum_{k_1=-\infty}^{\infty}a_{I\mu}^{(k_1)}a_{Sv}^{(k-k_1)} \tag{13}$$

where μ, ν are either x or y. Some of the $a_\mu^{(k)}$ and $a_\nu^{(k)}$ Fourier coefficients are plotted in Fig. S2 of the Supporting Information as a

function of k under the assumption that $\omega_{1I} = \omega_{1S}$ for values of $\omega_1/\omega_m = 1.0$ and 1.2.

In the CPPI experiment, the conditions $\omega_{1I} = \omega_{1S} = \omega_1$ and $\Delta\omega_{1S} = 2\omega_r$ are fulfilled while the modulation frequency ω_m is arbitrary. This leads to the resonance condition

$$n_0\omega_r \pm \frac{\Delta\omega_{1S}}{2} = 0 \tag{14}$$

with $n_0 = \pm 1$ and, as a consequence of the parameters used in the experiment, we find $a_I^{(k)} = a_S^{(k)}$ and $b_I^{(k)} = b_S^{(k)}$. The first-order effective Hamiltonian on the resonance condition is then given by

$$\begin{aligned}\overline{\mathscr{H}}^{(1)} &= \widetilde{\mathscr{H}}^{(1,0,-1)} + \widetilde{\mathscr{H}}^{(-1,0,1)} \\ &= -\frac{1}{2}\sum_p \left(a_S^{(0)*}\omega_{S_p}^{(+1)}S_p^- + a_S^{(0)}\omega_{S_p}^{(-1)}S_p^+\right) \\ &\quad + \sum_{d,p}\omega_{S_pI_d}^{(+1)}S_p^-\left[I_{dx}\left(b_{xx}^{(0)} - ib_{xy}^{(0)}\right) - I_{dy}\left(b_{yx}^{(0)} - ib_{yy}^{(0)}\right)\right] \\ &\quad + \sum_{d,p}\omega_{S_pI_d}^{(-1)}S_p^+\left[I_{dx}\left(b_{xx}^{(0)} + ib_{xy}^{(0)}\right) - I_{dy}\left(b_{yx}^{(0)} + ib_{yy}^{(0)}\right)\right]\end{aligned} \tag{15}$$

The expression of Eq. (15) can be simplified since the b_{xy}^0 and b_{yx}^0 are usually small or even zero for integer ratios of ω_1 and ω_m (see Fig. S1 of the Supporting Information)

$$\begin{aligned}\overline{\mathscr{H}}^{(1)} &= -\frac{1}{2}\sum_p \left(a_S^{(0)*}\omega_{S_p}^{(+1)}S_p^- + a_S^{(0)}\omega_{S_p}^{(-1)}S_p^+\right) \\ &\quad + \sum_{d,p}\omega_{S_pI_d}^{(+1)}S_p^-\left[I_{dx}b_{xx}^{(0)} + I_{dy}ib_{yy}^{(0)}\right] + \omega_{S_pI_d}^{(-1)}S_p^+\left[I_{dx}b_{xx}^{(0)} - I_{dy}ib_{yy}^{(0)}\right]\end{aligned} \tag{16}$$

Assuming in addition that $b_{xx}^{(0)} = b_{yy}^{(0)}$=0.5 and $a_x^{(0)} = 0$ which is fulfilled for integer ratios of ω_1 and ω_m (see Fig. S1 of the Supporting Information), we obtain

$$\begin{aligned}\overline{\mathscr{H}}^{(1)} &= \frac{i}{2}a_y^{(0)}\sum_p\left(\omega_{S_p}^{(+1)}S_p^- - \omega_{S_p}^{(-1)}S_p^+\right) \\ &\quad + \frac{1}{2}\sum_{d,p}\left(\omega_{S_pI_d}^{(+1)}S_p^-I_d^+ + \omega_{S_pI_d}^{(-1)}S_p^+I_d^-\right)\end{aligned} \tag{17}$$

which is in essence a rotary-resonance recoupling Hamiltonian [46,47] for the CSA tensors and a zero-quantum recoupling Hamiltonian on the heteronuclear dipolar coupling. Note, that for non-integer ratios of ω_1 and ω_m, the Hamiltonian will be a mixed zero-quantum and double-quantum Hamiltonian since $b_{xx}^{(0)} \neq b_{yy}^{(0)}$ under these conditions.

The phase-inverted CP experiment as implemented previously [5] with the amplitude jump on the S spins leads to a simultaneous dephasing of the S-spin magnetization under the heteronuclear dipolar coupling and the S-spin CSA tensor. The evolution under the full Hamiltonian of Eq. (17) cannot be calculated analytically but neglecting the CSA tensor we obtain a dephasing of the S-spin magnetization by a single heteronuclear dipolar coupling described by $\cos^2\left(\frac{1}{2}\left|\omega_{SI}^{(+1)}\right|t\right)$. Moving the amplitude jump to the passive spins would have the advantage that the dephasing by the CSA tensor will only enter as a second-order effect. The spin-locking properties for such an experiment, however, are only good if the rf-field amplitude is an integer multiple of the modulation frequency (see also Fig. 9 below). This can be seen from Eq. (12) since the non-resonant contribution to the effective Hamiltonian ($\widetilde{\mathscr{H}}^{(0,0,0)}$) contains isotropic chemical-shift terms that are scaled by $a_{Ix}^{(0)}$ and $a_{Iy}^{(0)}$. These scaling factors are zero for integer ratios of ω_1 and ω_m. Otherwise an additional oscillation under the scaled isotropic chemical shift can be observed which makes data evaluation difficult. Due to the fact that the rf-field amplitude on one of the spins has to be changed by $2\omega_r$, the phase-inverted CP experiment is only applicable for slow to intermediate MAS frequencies.

2.3. Symmetry-based RN_n^v sequences

Symmetry-based pulse sequences [25,48–50] can be used to generate effective Hamiltonians by selecting terms of the full spin-system Hamiltonian that have certain properties under rotations in spin space and real space. Such sequences can be analyzed using bimodal Floquet theory [44,51]. The interaction-frame transformation for the RN_n^v sequence on the I spins is given by

$$U(t) = \hat{T}\exp\left(i\int_0^t \omega_{1I}\sum_e(\cos(\phi(t'))I_{ex} + \sin(\phi(t'))I_{ey})dt'\right) \tag{18}$$

where $\hat{T}$ is the Dyson time-ordering operator [52] which ensures the proper time ordering of non-commuting propagators in products. The interaction-frame Hamiltonian has two independent frequencies and can be written as

$$\widetilde{\mathscr{H}}(t) = \sum_{n=-2}^{2}\sum_{k=-\infty}^{\infty}\widetilde{\mathscr{H}}^{(n,k)}e^{in\omega_r t}e^{ik\omega_m t} \tag{19}$$

where the basic frequency $\omega_m = 2\pi/\tau_m$ depends on the cycle time $\tau_m = n\tau_r$ of the RN_n^v sequence. The Fourier coefficients of the Hamiltonian are given by

$$\begin{aligned}\widetilde{\mathscr{H}}^{(0,k)} &= \left\{\sum_{d<e}\omega_{I_dI_e}^{(0)}2\vec{I}_d\cdot\vec{I}_e + \sum_{p<q}\omega_{S_pS_q}^{(0)}2\vec{S}_p\cdot\vec{S}_q + \sum_p\omega_{S_p^{(0)}}S_{pz}\right\}\delta_{k,0} \\ &\quad + \sum_d\omega_{I_d}^{(0)}\sum_{s=-1}^{1}a_{1,s}^{(k)}T_{1,s}^{(d)} + \sum_{p,d}\omega_{I_dS_p}^{(0)}2S_{pz}\sum_{s=-1}^{1}a_{1,s}^{(k)}T_{1,s}^{(d)}\end{aligned}$$

$$\begin{aligned}\widetilde{\mathscr{H}}^{(n,k)} &= \left\{\sum_{p<q}\omega_{S_pS_q}^{(n)}(3S_{pz}S_{qz} - \vec{S}_p\cdot\vec{S}_q) + \sum_p\omega_{S_p}^{(n)}S_{pz}\right\}\delta_{k,0} \\ &\quad + \sum_{d<e}\sqrt{6}\omega_{I_dI_e}^{(n)}\sum_{s=-2}^{2}a_{2,s}^{(k)}T_{2,S}^{(d,e)} + \sum_d\omega_{I_d}^{(n)}\sum_{s=-1}^{1}a_{1,s}^{(k)}T_{1,s}^{(d)} \\ &\quad + \sum_{p,d}\omega_{I_dS_p}^{(n)}2S_{pz}\sum_{s=-1}^{1}a_{1,s}^{(k)}T_{1,s}^{(d)}\end{aligned} \tag{20}$$

where $n \neq 0$. Here we have used the spherical-tensor notation for the I spins with

$$\begin{aligned}T_{1,0}^{(d)} &= I_{dz} \\ T_{1,\pm1}^{(d)} &= \frac{\mp1}{\sqrt{2}}I_d^\pm\end{aligned} \tag{21}$$

and

$$\begin{aligned}T_{2,0}^{(d,e)} &= \frac{1}{\sqrt{6}}[3I_{dz}I_{ez} - (\vec{I}_d\cdot\vec{I}_e)] \\ T_{2,\pm1}^{(d,e)} &= \mp\frac{1}{2}\left[I_d^\pm I_{ez} + I_{dz}I_e^\pm\right] \\ T_{2,\pm2}^{(d,e)} &= \frac{1}{2}\cdot\left[I_d^\pm I_e^\pm\right]\end{aligned} \tag{22}$$

The Fourier coefficients $a_{l,s}^{(k)}$ of the interaction-frame transformation of the $T_{2,0}^{(d,e)}$ and $T_{1,0}^{(d)}$ operators are defined by

$$a_{l,s}(t) = \sum_k a_{l,s}^{(k)}e^{ik\omega_m t} \tag{23}$$

The values of the $a_{l,s}^{(k)}$ coefficients can be calculated numerically and depend on the parameters of the RN_n^v sequence. For an RN_n^v pulse sequence, the condition for non-zero values of the Fourier coefficients $a_{l,s}^{(k_0)}$ is given by

$$k_0 = \frac{zN}{2} - sv \tag{24}$$

where z is an integer with the same parity as l, i.e., z is odd if l is odd and z is even if l is even. Analytical expressions for the Fourier coefficients $a_{l,s}^{(k_0)}$ can be found in Ref. [51] or they can be calculated numerically by a Fourier transformation of the interaction-frame trajectories (see Figs. S3 and S4 of the Supporting Information).

On the first-order resonance conditions with $n_0\omega_r + k_0\omega_m = 0$ the non-zero parts of the Fourier coefficients $\widetilde{\mathscr{H}}^{(n_0,k_0)}$ are recoupled. Since $\omega_r = n\omega_m$ for any RN_n^v sequence, the resonant terms are given by $\widetilde{\mathscr{H}}^{(n_0,-nn_0)}$ with $n_0 = \pm1$ or ±2. For recoupling of the heteronuclear dipolar couplings, the $R18_2^5$ and $R18_1^7$ sequences have been proposed [6,27,26] using a simple 180° pulse as the basic R element. The rf-field requirement for the two pulse sequences is $\omega_1 = 4.5\omega_r$ and $9\omega_r$, respectively, which makes them suitable for slow to intermediate MAS frequencies. For fast MAS, a different sequence would be required with a lower ratio of rf-field amplitude and spinning frequency.

For the $R18_2^5$ and $R18_1^7$ sequences, $n = 2$ and 1. This implies that only terms with non-vanishing Fourier coefficients $a_{l,s}^{k_0}$ with $k_0 = \pm2$ or ±4 can be recoupled by the $R18_2^5$ sequence and terms with $k_0 = \pm1$ or ±2 can be recoupled by the $R18_1^7$ sequence. Only the $a_{1,\pm1}^{(\pm4)}$ terms for the $R18_2^5$ sequence and the $a_{1,\pm1}^{(\pm2)}$ terms for the $R18_1^7$ fulfill this condition (see Figs. S3 and S4 in the Supplementary Material) leading to first-order effective Hamiltonians of the form

$$\begin{aligned}\overline{\mathscr{H}}^{(1)} &= \widetilde{\mathscr{H}}^{(+2,-4)} + \widetilde{\mathscr{H}}^{(-2,+4)} \\ &= \frac{\left|a_{1,-1}^{(-4)}\right|}{\sqrt{2}} \sum_d \left(\omega_{I_d}^{(+2)} I_d^- + \omega_{I_d}^{(-2)} I_d^+\right) \\ &\quad + \frac{\left|a_{1,-1}^{(-4)}\right|}{\sqrt{2}} \sum_{p,d} \left(\omega_{I_d S_p}^{(+2)} 2S_{pz} I_d^- + \omega_{I_d S_p}^{(-2)} 2S_{pz} I_d^+\right)\end{aligned} \tag{25}$$

and

$$\begin{aligned}\overline{\mathscr{H}}^{(1)} &= \widetilde{\mathscr{H}}^{(+2,-2)} + \widetilde{\mathscr{H}}^{(-2,+2)} \\ &= \frac{\left|a_{1,-1}^{(-2)}\right|}{\sqrt{2}} \sum_d \left(\omega_{I_d}^{(+2)} I_d^- + \omega_{I_d}^{(-2)} I_d^+\right) \\ &\quad + \frac{\left|a_{1,-1}^{(-2)}\right|}{\sqrt{2}} \sum_{p,d} \left(\omega_{I_d S_p}^{(+2)} 2S_{pz} I_d^- + \omega_{I_d S_p}^{(-2)} 2S_{pz} I_d^+\right)\end{aligned} \tag{26}$$

respectively. The coefficients $a_{1,-1}^{(-4)} \approx 0.4253$ and $a_{1,-1}^{(-2)} \approx 0.4395$ leading to a scaling factor of the $R18_2^5$ sequence of $\kappa = \sqrt{2}\left|a_{1,-1}^{(-4)}\right| \approx 0.602$ and for the $R18_1^7$ sequence of $\kappa = \sqrt{2}\left|a_{1,-1}^{(-2)}\right| \approx 0.622$. In both cases, the I-spin CSA tensor is recoupled with the same efficiency. For a single heteronuclear dipolar coupling, the dephasing of the S-spin magnetization is described by $\cos\left(\kappa\left|\omega_{IS}^{(+2)}\right|t\right)$ while the recoupled I-spin CSA tensor enters only indirectly. This corresponds to a scaling of the width of the powder pattern (measured between the two singularities at $\beta = 90°$) compared to the static case by 0.301 and 0.311, respectively.

2.4. T-MREV-N sequences

The transverse MREV sequences (T-MREV-*N*) [24,53] are a class of pulse sequences where the basic building block is a modified version of the MREV-8 cycle [54,55] for homonuclear decoupling which is then repeated N times within a rotor cycle and the phases of all pulses are shifted by $2\pi/N$ (Fig. 4). This can be viewed as a symmetry-based CN_1^1 sequence [25] where the basic C element is the modified MREV-8 cycle.

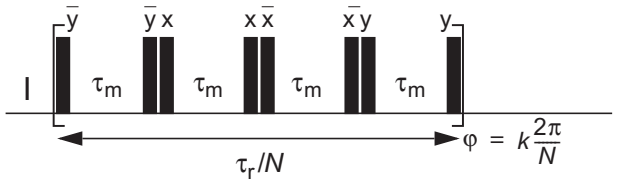

Fig. 4. Basic building block of the T-MREV-N pulse succulence with indications for the timing and phases of the pulses.

It is possible to calculate the first-order average Hamiltonian of the T-MREV-*N* pulse sequence under MAS using finite pulses in order to obtain the scaling factors of the heteronuclear dipolar couplings. Using a notation similar to the one used in the finite-pulse REDOR calculations with $\phi = \omega_r/\omega_1$ leads to a length of the 90° pulses of $\tau_p = \frac{\phi}{4}\tau_r$ and to a length of the delays between the pulses of $\tau_m = \left(\frac{1}{4N} - \frac{\phi}{2}\right)\tau_r$. This limits the range of ϕ to $0 \leqslant \phi < \frac{1}{2N}$ so that the delay τ_m is not vanishing. Assuming a high-field truncated heteronuclear dipolar-coupling Hamiltonian of the form

$$\mathscr{H}_{IS}(t) = 2I_zS_z \sum_{n=-2}^{2} \omega_{IS}^{(n)} e^{in\omega_r t} \tag{27}$$

we obtain for $N > 3$ a first-order average Hamiltonian of the form

$$\overline{\mathscr{H}}_{IS}^{(1)} = \left(\kappa\omega_{IS}^{(+1)} I^- + \kappa^*\omega_{IS}^{(-1)} I^+\right) S_z \tag{28}$$

The analytical expressions for κ have been calculated using Mathematica (Wolfram Research Inc., Champaign, IL, USA) as a function of N. They are a function of the pulse length and the rf-field amplitude. Fig. 5 shows a plot of κ as a function of ϕ for $N = 4$ to 8, which are almost linear functions of ϕ. The exact functional form is given by

$$\kappa = \frac{z_1\phi + z_2\cos\left(\frac{\pi\phi}{2}\right) + z_3\sin\left(\frac{\pi\phi}{2}\right)}{\pi(\phi^2 - 1)} \tag{29}$$

and numerical values for the parameters z_i are given in Table 1. The calculated scaling factors agree very well with powder patterns obtained from full numerical simulations of the T-MREV-*N* sequence using the GAMMA simulation package [56].

It is important to note that even in first-order AHT, the T-MREV-*N* sequences are not perfect homonuclear decoupling sequences. Starting from a homonuclear dipolar-coupling Hamiltonian of the form

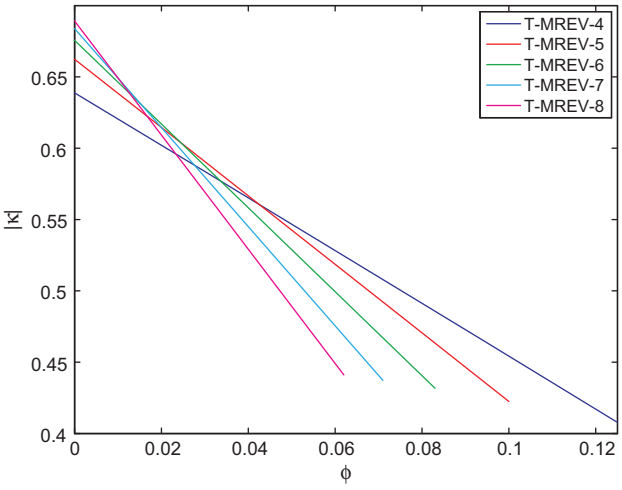

Fig. 5. Scaling factors κ for the T-MREV-*N* sequences as a function of the ratio $\phi = \omega_r/\omega_1$.

Table 1
Numerical values for the parameters of the scaling factor κ for the T-MREV-N sequences.

N	z_1	z_2	z_3
4	$-10.0547 + 0.8284i$	$-2.0000 + 0.1648i$	$10.0547 - 0.8284i$
5	$-12.8537 + 2.7195i$	$-2.0358 + 0.4307i$	$12.8537 - 2.7195i$
6	$-15.4169 + 4.7195i$	$-2.0297 + 0.6213i$	$15.4169 - 4.7195i$
7	$-17.8291 + 6.7580i$	$-2.0089 + 0.7614i$	$17.8291 - 6.7580i$
8	$-20.1416 + 8.8090i$	$-1.9838 + 0.8676i$	$20.1416 - 8.8090i$

$$\mathscr{H}_{\mathrm{II}}(t) = (2I_{1z}I_{2z} - (I_{1x}I_{2x} + I_{1y}I_{2y})) \sum_{n=-2}^{2} \omega_{\mathrm{II}}^{(n)} e^{in\omega_r t} \tag{30}$$

we find for the T-MREV-4 sequence even in the delta-pulse limit a first-order Hamiltonian of the form

$$\overline{\mathscr{H}}_{\mathrm{II}}^{(1)} = \frac{3(\sqrt{2}-1)}{\pi} \cdot \mathrm{Im}\left(\omega_{\mathrm{II}}^{(+2)}\right)(2I_{1y}I_{2y} - 2I_{1x}I_{2x}) \tag{31}$$

leading to a powder line with a width of approximately $\delta_{\mathrm{II}}/10$. For finite pulses the magnitude of the scaling factor is changed and additional two-spin terms appear but with much smaller coefficients. For the T-MREV-5 sequence one obtains in the delta-pulse limit a more complicated first-order AHT of the form

$$\begin{aligned}\overline{\mathscr{H}}_{\mathrm{II}}^{(1)} \approx{}& \left(0.1274 \cdot \mathrm{Re}\left(\omega_{\mathrm{II}}^{(+2)}\right) - 0.0414 \cdot \mathrm{Im}\left(\omega_{\mathrm{II}}^{(+2)}\right)\right)(2I_{1x}I_{2y} \\ &+ 2I_{1y}I_{2x}) \\ &+ \left(0.0414 \cdot \mathrm{Re}\left(\omega_{\mathrm{II}}^{(+2)}\right) + 0.1274 \cdot \mathrm{Im}\left(\omega_{\mathrm{II}}^{(+2)}\right)\right)(2I_{1y}I_{2y} \\ &+ 2I_{1x}I_{2x})\end{aligned} \tag{32}$$

For finite pulses the scaling factors change and additional terms appear. T-MREV-N sequences with higher values of N are also not perfect homonuclear decoupling sequences even in first-order AHT and assuming delta pulses.

The design of the pulse sequence limits the application to slow MAS frequencies since the requirement for the rf-field amplitude is $\omega_1 > 2N\omega_r$. Since $N > 3$ is required for the T-MREV sequences [24,53], spinning frequencies above 15–20 kHz require very strong rf fields. Preferably, even lower spinning frequencies should be used to obtain better scaling factors for the heteronuclear dipolar couplings. For $N = 2$ and $N = 3$, the Hamiltonian has a different form. For $N = 2$, the T-MREV pulse sequence recouples only the $\omega_{\mathrm{IS}}^{(\pm1)}$ component but is no longer γ encoded while for $N = 3, \omega_{\mathrm{IS}}^{(\pm1)}$ and $\omega_{\mathrm{IS}}^{(\pm2)}$ are both recoupled.

3. Numerical simulations

In order to compare the performance of the four different pulse sequences shown in Fig. 1 numerical simulations were performed using the software package GAMMA [56]. In the following, we will focus primarily on ^{15}N–^{1}H spin pairs, but all conclusions can directly be transferred to other X–^{1}H systems. It is the aim of these simulations to provide a quantitative measure of the sensitivity of the different pulse sequences to experimental imperfections and to additional terms in the spin-system Hamiltonian which have been neglected in the analytical treatment, e.g., CSA tensors or additional "remote" proton spins. As a measure for such systematic effects, the deviation of the effective dipolar-coupling anisotropy $\delta_{\mathrm{IS}}^{\mathrm{eff}}$ extracted from such simulations from the nominal value of the dipolar coupling δ_{IS} was used.

3.1. Computational parameters and methods

A set of test simulations was performed with different CSA parameters, remote spins, and rf-field amplitude settings assuming a fixed anisotropy of the ^{15}N–^{1}H dipolar coupling $\delta_{\mathrm{IS}}/(2\pi) = 19.5$ kHz. This corresponds to an effective N–H bond length of 1.077 Å. The data evaluation was based on a set of ideal two-spin simulations with fixed standard CSA parameters and ideal rf-field amplitudes and pulse lengths, varying $\delta_{\mathrm{IS}}/(2\pi)$ in the range of 14 to 36 kHz in steps of 10 Hz. The latter simulations were used for fitting the test simulations to extract the apparent value of the dipolar-coupling anisotropy $\delta_{\mathrm{IS}}^{\mathrm{eff}}$ from the test simulations.

Unless otherwise noted, the following standard parameters were used in all simulations: ^{1}H CSA $\sigma_{zz} = 2$ ppm, $\eta = 0$, inclined relative to the H–N internuclear vector at 10°; ^{15}N CSA $\sigma_{zz} = 113$ ppm, $\eta = 0$, inclined relative to the H–N internuclear vector at 20°, at a B_0 field of 14.1 T corresponding to a proton Larmor frequency of 600 MHz. This is a typical situation for a ^{15}N CSA tensor in a peptide. Powder averaging was implemented according to the ZCW scheme [57] using 2500 or 10,000 powder points for the two-spin and the three-spin simulations, respectively. The following MAS und pulse settings were used for the T-MREV-N simulations: MAS 9.47 kHz ($\tau_r = 105.6$ µs), corresponding to a 90° pulse length of 2.2 µs using the T-MREV-4 scheme ($\omega_1 = 3N\omega_r$). The nominal ideal ^{1}H rf-field amplitude is $\nu_1 = 113.636$ kHz. In the $\mathrm{R18}_1^7$ ($\mathrm{R18}_2^5$) simulations the MAS frequency was 10 kHz (20 kHz), corresponding to a ^{1}H rf field of $\nu_1 = 90$ kHz in both cases. The phase-inverted CP (CPPI) experiment was simulated at 20 kHz MAS, employing the amplitude and phase alternations required for jumping from the +1 to the −1 Hartmann–Hahn match every 10 µs, similar to previous measurements [5]. The rf-amplitude jumps from $\nu_1 = 36$ kHz to 76 kHz were employed either on the ^{1}H spins (referred to as "jump H") or on the ^{15}N spins ("jump N"), while the rf-field amplitude on the other channel was kept constant at 56 kHz. In all REDOR simulations the ^{1}H and ^{15}N 180° pulses were 4 µs and 10 µs, respectively, corresponding to rf-field amplitudes of $\nu_1 = 125$ kHz and 50 kHz. The REDOR experiment was simulated at MAS frequencies of 20 and 50 kHz. The shift of the pulses τ_s was 20.5 µs ($\varepsilon = 0.82$) or 13.75 µs ($\varepsilon = 0.55$) at 20 kHz and 5.5 µs at 50 kHz MAS ($\varepsilon = 0.55$). The choice of the MAS frequencies was motivated by the following considerations: in the case of REDOR, high MAS frequencies are readily accessible without the need for very high rf fields, while MAS frequencies above 10 to 15 kHz are inaccessible to T-MREV-N and $\mathrm{R18}_1^7$, and MAS frequencies above about 30 kHz are inaccessible to $\mathrm{R18}_2^5$. The CPPI experiment requires jumps of the rf amplitude of $2\omega_r$, which becomes also very challenging for MAS frequency above 30–40 kHz.

Extraction of the apparent dipolar-coupling $\delta_{\mathrm{IS}}^{\mathrm{eff}}$ from the test simulations was done using the data of the first 3 ms of the time evolution under the recoupling sequences. For the REDOR experiment, all recoupling curves were first translated into normalized REDOR curves, by calculating $\Delta S/S_0$. The apparent dipolar coupling was then obtained from a fit of the ideal two-spin simulation to the simulated data sets by finding the one with the lowest χ^2 value. Extraction of the apparent dipolar coupling $\delta_{\mathrm{IS}}^{\mathrm{eff}}$ from the data of the T-MREV-N and the $\mathrm{R18}_n^{\nu}$ sequences was also performed using time-domain data. However, two additional parameters were needed, an offset and a scaling factor for the absolute intensity. For each ideal two-spin simulation, these two parameters were optimized individually and the ideal two-spin simulation with the lowest χ^2 value to the test simulations data was selected, leading to the apparent dipolar coupling $\delta_{\mathrm{IS}}^{\mathrm{eff}}$. We have also repeated this fitting procedure with a third fit parameter that describes an exponential damping. The results in terms of the extracted $\delta_{\mathrm{IS}}^{\mathrm{eff}}$ are identical, except for the case of rf field-distributions (see

Table 2
Relative deviations of δ_{IS}^{eff} from the real δ_{IS} obtained from fitting 3 ms of recoupling.

	TMREV (%)	$R18_2^5$ (%)	$R18_1^7$ (%)	REDOR 20 kHz (%)	REDOR 50 kHz (%)
Scenario 1: half-gaussian of width 6% towards lower and 2% towards higher fields					
2-spin	+2.6	+2.8	+2.7	−0.2	−1.3
3-spin system 1	+2.7	+3.2	+2.9	<0.2	−0.5
3-spin system 2	+3.2	+3.3	+2.9	+1.2	+0.5
Scenario 2: half-gaussian of width 10% towards lower and 4% towards higher fields					
2-spin	+2.0	+3.3	+2.7	−0.2	−2.1
3-spin system 1	+2.1	+3.4	+3.0	+0.2	−1.3
3-spin system 2	+2.7	+3.5	+3.0	+1.3	−0.4

Table 2), where the three-parameter model was used. The apparent dipolar couplings obtained from the time-domain data very closely match the couplings obtained from analyzing the frequency-domain data of the T-MREV-N and $R18_n^\nu$ simulations. For the CPPI experiment, a time-domain fit was not possible, because of a low-frequency modulation of the magnetization due to the ^{15}N CSA, which dominates the signal in the time domain (see Fig. 6d). We, thus, obtained the apparent dipolar coupling δ_{IS}^{eff} from the CPPI test simulations by comparing the observed peak splitting in the frequency domain with the splitting in ideal two-spin simulations, equal to the procedure outlined in a recent study [5]. Again, the Fourier transform of the data for the first 3 ms of the mixing time were used for this analysis.

3.2. Sensitivity to amplitude missettings and inhomogeneities in the rf field

The simulations in Fig. 6 illustrate the sensitivity of the different experimental approaches to missetting of the ^1H rf-field amplitude.

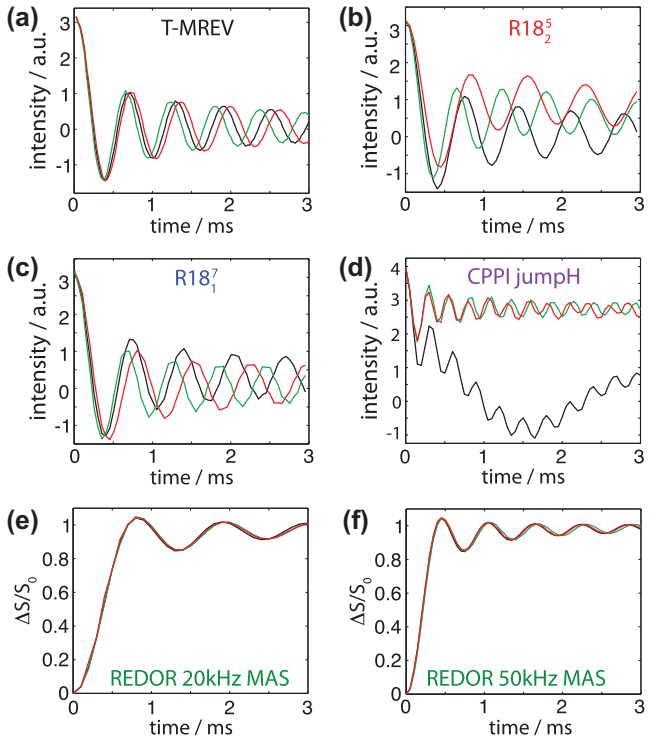

Fig. 6. The effect of ^1H rf-field miscalibration on the recoupling behavior in the different simulations, (a) T-MREV-N, (b) $R15_2^5$, (c) $R15_1^7$, (d) CPPI with alternation of the ^1H rf-field amplitude, and REDOR at (e) 20 kHz MAS with τ_s = 13.75 μs and (f) 50 kHz MAS with τ_s = 5.5 μs (i). Shown are simulations using the correct ^1H rf-field amplitude (black) as well as a 9% too low (green) and 9% too high (red) rf amplitude. (For interpretation of the references to colour in this figure legend, the reader is referred to the web version of this article.)

Time traces for all experiments at ideal ^1H rf-field amplitudes (black) are shown, as well as for amplitudes that are 9% too low (green) and 9% too high (red). On a qualitative level, the four pulse sequences show clear differences in the sensitivity to ^1H rf-field missettings. The T-MREV-*N* and the $R18_2^5$ sequences show larger dipolar oscillation frequencies for too low rf-field amplitudes, and smaller oscillation frequencies for too high rf-field amplitudes. Furthermore, a significant zero-frequency offset (Fig. 6b) is observed for the $R18_2^5$ sequence [6,27].

When considering the outcome of the CPPI-jumpH experiment as a function of the ^1H rf-field amplitude, it has to be realized that there are two different ^1H rf field strengths that have to be set to match the n = +1 and −1 Hartmann–Hahn condition, respectively. Accordingly, these two different rf fields can be set (and mis-set) independently, resulting in a two-dimensional parameter space to be investigated. In a recent study it was assumed that the two rf fields are mis-set by the same absolute amount [5]. In this case, the experiment was reported to be rather robust to this amount of rf field mis-setting. We have simulated different situations, where the two ^1H rf fields are mis-set by different absolute amounts. In all cases we observe a pronounced dependence of the oscillation frequency on the settings. In the following, we focus here on the scenario where the two ^1H rf fields are misset by the same *relative* amount. This situation is relevant when considering the effects of rf field inhomogeneity. In Fig. 6d we assumed that the relative missetting is equal for the n = +1 and −1 Hartmann–Hahn match, once both fields are 9% above the nominal field strength, and in one case 9% below. Interestingly, and in contrast to the T-MREV-*N* and $R18_2^5$ sequences, the apparent dipolar coupling is too high in both cases. In fact, in all simulated cases with misset rf-field amplitudes we find too fast oscillation frequencies. We also note that the CPPI-jumpN experiment is largely insensitive to missetting of the ^1H rf

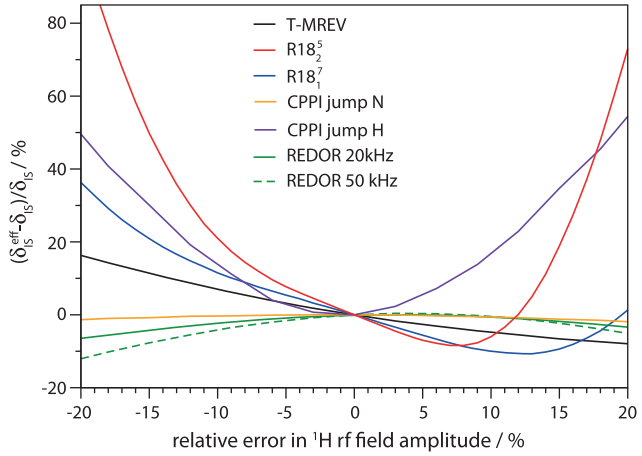

Fig. 7. Relative deviation of the fitted dipolar-coupling asymmetry δ_{IS}^{eff} from the value of 19.5 kHz entered into the simulation, as a function of the ^1H rf-field amplitude relative to the corresponding nominal value.

field but sensitive to missettings of the ^{15}N field, while the opposite is true for CPPI-jumpH (vide infra). A visual inspection of the REDOR data of Fig. 6e and f shows that the REDOR experiment is only very weakly sensitive to rf-field missettings.

The apparent dipolar coupling δ_{IS}^{eff}, as extracted for the simulated curves of Fig. 6 and further simulations are given in Fig. 7 as a function of the ^{1}H rf-field error. There are clear differences in the sensitivity of the pulse schemes to errors in the rf-field amplitude. The weakest sensitivity, i.e., the most accurate dipolar couplings as a function of the ^{1}H rf-field setting, are found for the REDOR and the CPPI-jumpN experiment. Fig. 8 shows the same analysis for errors in the ^{15}N rf-field amplitude for the sequences that require ^{15}N irradiation (REDOR and CPPI). Here, a strong dependence of the apparent dipolar coupling is observed for the CPPI-jumpN experiment while the REDOR is only very weakly influenced.

In a realistic experimental setup, one generally does not only face a simple missetting of the rf field from the nominal value to another discrete value, but rather a distribution of rf fields across the rf coil volume. This situation will be considered together with the influence of remote proton spins below.

3.3. Sensitivity to carrier offset and chemical-shift distributions

Isotropic chemical-shift offsets from the rf carrier frequency are another possible source of errors that must be considered. Our simulations show, however, that the effect of chemical-shift offsets is negligible in all experiments, except for the CPPI experiment. Fig. 9 shows the sensitivity of the CPPI-jumpH and CPPI-jumpN experiments to ^{1}H and ^{15}N frequency offsets. The CPPI-jumpH experiment is sensitive to offset of the ^{15}N frequency, while the outcome of the jumpN experiment depends on the frequency of the ^{1}H nucleus relative to the rf carrier position. This is due to the feature that the CPPI experiment has no effective spin-lock component on the channel where only phase inversions and no amplitude jumps occur. Under such a phase-alternating irradiation, isotropic chemical-shift offsets are only averaged out if the nutation frequency ω_1 is an integer multiple of the modulation frequency ω_m as pointed out in the Theory section. To illustrate this, we have simulated a number of different ^{1}H rf fields, from 50 to 100 kHz, using a pulse element length of $\tau_m/2 = 10$ μs and ensuring Hartmann–Hahn match by adjusting the rf fields on the ^{15}N channel accordingly. If the rf field amplitude is matched such that an integer multiple of a full 2π nutation is achieved within the pulse

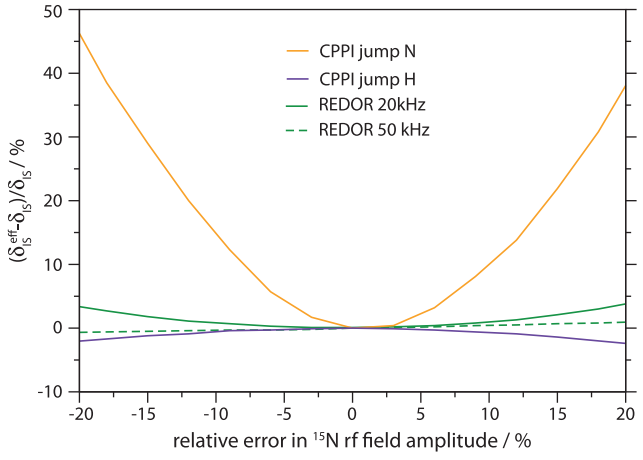

Fig. 8. Relative deviation of the fitted dipolar-coupling asymmetry δ_{IS}^{eff} from the true value of 19.5 kHz as a function of the ^{15}N rf-field amplitude shown for CPPI and REDOR simulations.

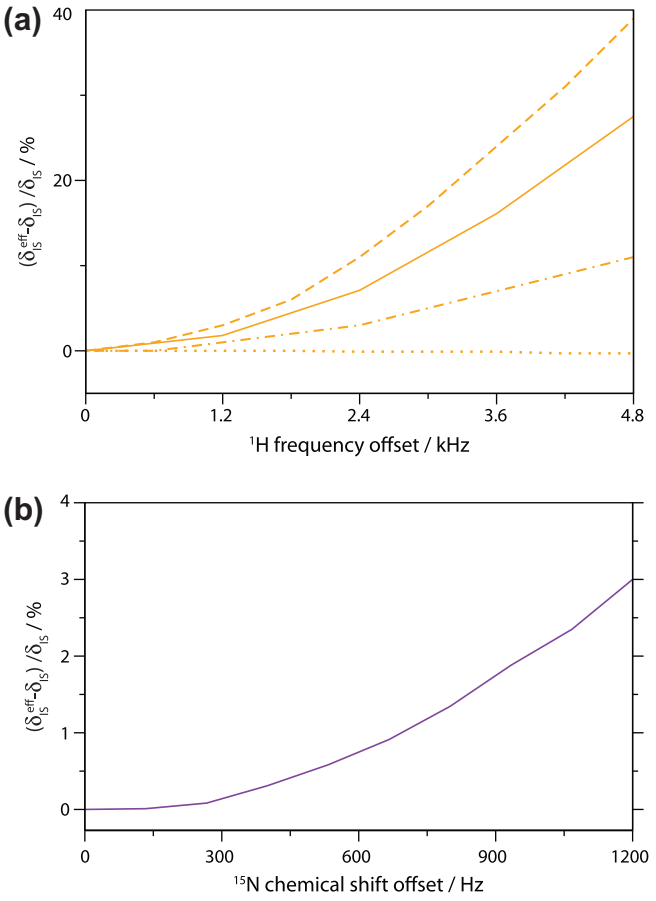

Fig. 9. Dependence of the apparent dipolar coupling δ_{IS}^{eff} on chemical shift offsets of ^{1}H (a) and ^{15}N (b). Shown are only data fort he CPPI experiment (jumpN in (a), jumpH in (b)), because in all other experiments the deviations due to chemical shift offsets are below 1% over this range of offsets. In (a) we show different implementations of the CPPI-jumpN experiment, with different rf field settings: dashed line: $\nu_1(^1H) = 50$ kHz, $\nu_1(^{15}N) = 30/70$ kHz; solid line: $\nu_1(^1H) = 56$ kHz, $\nu_1(^{15}N) = 36/76$ kHz; dot-dashed line: $\nu_1(^1H) = 75$ kHz, $\nu_1(^{15}N) = 55/95$ kHz; dotted line: $\nu_1(^1H) = 100$ kHz, $\nu_1(^{15}N) = 80/120$ kHz. In (b) is shown the CPPI-jumpH experiment with $\nu_1(^1H) = 56$ kHz, $\nu_1(^{15}N) = 36/76$ kHz. In all cases, the phase/amplitude jumps are performed every 10 μs, i.e. $\tau_m/2 = 10$ μs.

duration of 10 μs (e.g. at 100 kHz ^{1}H rf field amplitude), the dependence of the apparent splitting on the ^{1}H frequency offset vanishes (dotted line in Fig. 9a). The strongest dependence on the ^{1}H frequency offset is found when the rf field amplitude is set to 50 kHz (dashed line), when only a π nutation is achieved during the duration of the pulse. It should be noted that in practice it is straightforward to take into account the effects of isotropic chemical-shift offsets when determining δ_{IS}, because rf carrier positions and resonance frequencies are known. Accordingly, when analyzing data recorded with the CPPI experiment, one can take this offset into account for each resonance to be analyzed by performing a set of simulations for each resonance peak separately when fitting the data [5].

3.4. Sensitivity to CSA tensors

Although CSA tensor parameters can, in principle, be measured in separate experiments [58,59], often a considerable uncertainty about the values remain and site-to-site variations of CSA parameters may be substantial, making the CSA, thus, a potential source of uncertainty in the determination of δ_{IS}. Fig. 10 shows the sensitivity of the dipolar-coupling measurement to CSA parameters. The anisotropy of the ^{1}H CSA tensor can generally be ignored over the

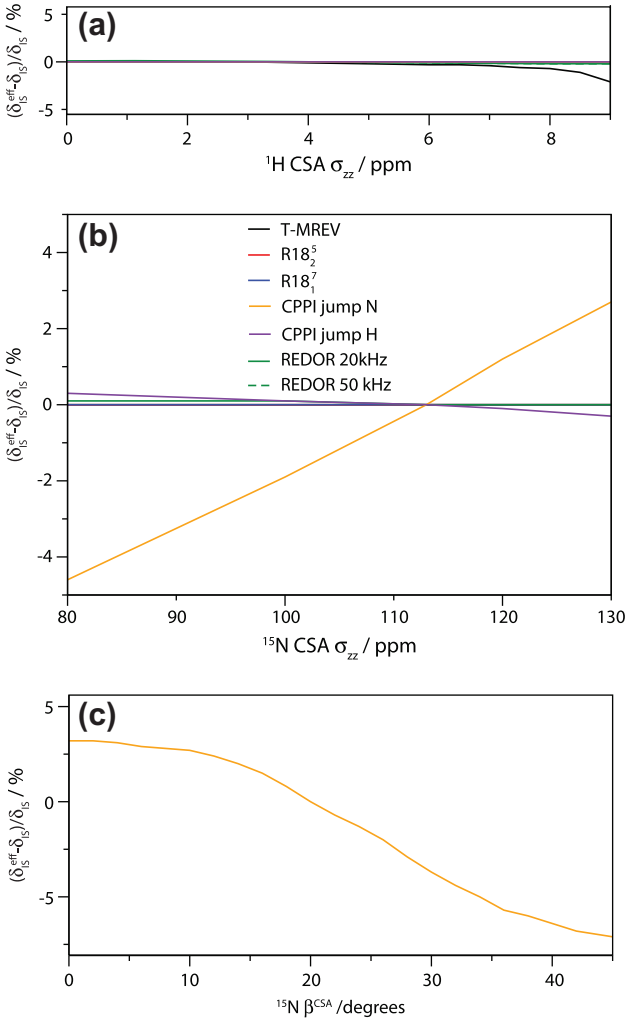

Fig. 10. Dependence of the fitted δ_{IS}^{eff} on the CSA of ^{1}H (a) and ^{15}N (b), as well as on the angle between the axially symmetric ^{15}N CSA tensor and the N–H dipolar tensor (c).

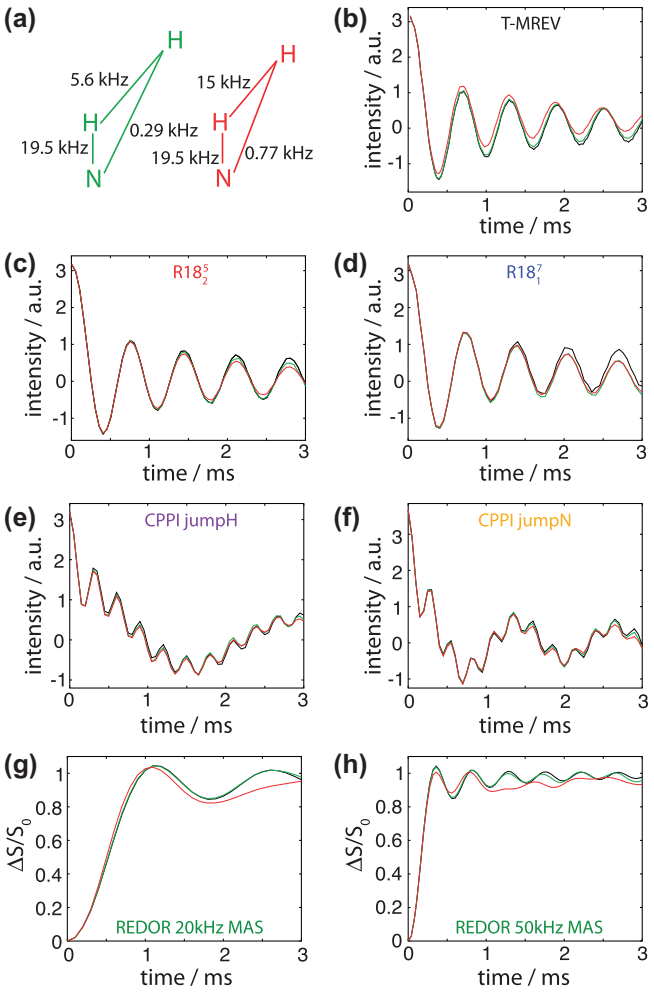

Fig. 11. Numerical simulation of the effect of an additional ^{1}H spin on the recoupling curves. Black: two-spin system; red: H–H–N three-spin system with the following couplings: H–H 15 kHz, H–N 770 Hz; green: H–H 5.6 kHz, H–N 290 Hz. Angles: N–H–H = 130° H–N–H = 76°. (For interpretation of the references to colour in this figure legend, the reader is referred to the web version of this article.)

relevant range of ^{1}H CSA values [60]. The ^{15}N CSA tensor has a substantial influence only in the CPPI jumpN experiment, as reported previously since it is actively recoupled by the constant part of the rf as shown in the Theory section. For the case of ^{15}N sites in the protein backbone, consensus values of σ_{zz} = 113 ppm and an angle of 10–25° between the N–H vector and the symmetry axis of the CSA have been established [1,61,62]. In the presence of sizeable dynamics, however, the chemical-shift anisotropy will be reduced. Inspection of Fig. 10 reveals that in such a situation the extracted value of δ_{IS}^{eff} from the CPPI-jumpN experiment slightly underestimates the true value of δ_{IS}. The dependence of the CPPI experiment on the ^{15}N CSA is a drawback of this method.

3.5. Sensitivity to couplings to extraneous proton spins

As a last source of errors, the presence of additional ^{1}H spins will be considered. Experimentally, effects from remote ^{1}H spins can most easily be avoided by preparing highly deuterated samples where only exchangeable hydrogen positions are populated by ^{1}H, while non-exchangeable sites are labeled with ^{2}H spins. However, even in such highly deuterated samples, distances between amide-hydrogen nuclei in protein β-sheets can be of the order of 2.5–4 Å, corresponding to a dipolar coupling δ_{IS} of approximately 4–15 kHz. Therefore, it is important to investigate the potential role of remote proton spins. Fig. 11 shows time-domain data for two-spin simulations (black), and two different three-spin simulations with a coupling of the two protons of $\delta_{IS}/(2\pi)$ = 15 kHz (red) and 5.6 kHz (green) and a coupling between the remote proton and the ^{15}N nucleus of 770 and 290 Hz (Fig. 11a). The Fourier transforms of these data are shown in Fig. S6 of the Supporting Information. The simulation using a 15 kHz ^{1}H–^{1}H coupling is a worst-case scenario for the measurement of amide N–H couplings in deuterated, back-exchanged proteins, as this corresponds roughly to the shortest amide-amide proton distance found in proteins. As seen from these data, the dipolar oscillations observed in the frequency domain data of T-MREV-*N*, R18$_2^5$ and CPPI is relatively insensitive to the presence of the additional ^{1}H spin.

In the REDOR experiment, the additional proton spin is readily observed in the time domain data. This is a consequence of the fact that the REDOR pulse sequence does not suppress homonuclear dipolar couplings and is not susceptible to dipolar-truncation effects (see Theory part). Table 3 lists the apparent dipolar couplings obtained for these three-spin systems under the different pulse sequences, using the same fitting procedures as used for the two-spin data. While in most cases the error introduced by the remote spin is below 0.5%, it is of note that in the REDOR experiment the errors are somewhat more substantial, and the extracted dipolar

Table 3
Relative deviations of δ_{IS}^{eff} from δ_{IS} in three-spin H–H–N systems.

	TMREV (%)	$R18_2^5$ (%)	$R18_1^7$ (%)	CPPI jumpH (%)	CPPI jumpN (%)	REDOR 20 kHz (%)	REDOR 50 kHz (%)
Spin system 1	+0.2	<0.2	+0.2	<0.2	<0.2	+0.4	+0.7
Spin system 2	+0.6	<0.2	+0.2	<0.2	−0.3	+1.3	+1.7

couplings δ_{IS}^{eff} are overestimating the real δ_{IS} by up to 2% in the simulated three-spin system with the 15 kHz ^{1}H–^{1}H coupling. Interestingly, this overestimation of the dipolar coupling introduced by a remote spin somewhat compensates the general trend that REDOR measures too small couplings in the presence of ^{1}H rf-field missetting (Fig. 7).

In order to determine the limits of the REDOR experiment to additional nearby proton spins, we have carried out multi-spin simulations that are characteristic for deuterated and fully proton back-exchanged samples as well as for fully protonated samples (Fig. S7 of the Supporting Information). For deuterated and 100% proton back-exchanged samples, the five-spin simulations include only N–H protons (Fig. S7, green curves) and give almost identical results to the ideal two-spin simulations at MAS frequencies of 20 and 50 kHz while at 10 kHz MAS there are significant deviations. For fully protonated samples (Fig. S7, red curves) the six-spin simulations including the nearest proton spins show strong deviations from the ideal two-spin simulations indicating that the REDOR experiment is feasible in deuterated and 100% proton back-exchanged samples at higher MAS frequencies (20 kHz) while it will not work in fully protonated samples.

3.6. Summary of the sensitivity to experimental missettings and to additional terms in the hamiltonian

We conclude that the largest source of error in the determination of dipolar couplings come from deviations of the rf-field amplitude from the theoretical value. Accurate calibration of the rf fields is, therefore, of crucial importance, especially in $R18_2^5$ and CPPI sequences, where the introduced errors are substantial. In any realistic probe, significant B_1 inhomogeneity is present. The impact of rf field inhomogeneity depends strongly on the detailed geometry of the coil in a given probe, and it is difficult to make general statements. Nonetheless, we have analyzed two different situations for rf-field inhomogeneities. Typically, the rf-field distribution is broader towards lower rf-field amplitudes than towards higher amplitudes. We have accounted for this by assuming that the rf-field distribution can be described by two half-gaussian distributions of different width. We assume that the peak of this distribution is at the nominal ideal rf-field amplitude, which is certainly an optimistic assumption, and the conclusions below should, thus, be regarded as a favorable case estimation. In scenario 1, we assume the half-Gauss distribution towards lower fields to have a width of 6% (i.e. 6 kHz if the nominal field strength is 100 kHz), while the distribution to higher field amplitudes is described by a width of 2%. In scenario 2, we assume widths of 10% and 4%. In the case of the REDOR experiments, we assumed that the distribution on ^{1}H and ^{15}N has the same relative widths, with the peak maximum at the nominal field strengths. For the CPPI experiment, three different fields have to be matched, giving many possible parameters to be investigated. We prefer not to assume a particular scenario for the CPPI experiment, and leave the investigation of rf inhomogeneities out for this experiment. From Fig. 7, however, it is clear that any distribution or miscalibration of rf fields will lead to larger values of δ_{IS}^{eff}, such that the extracted δ_{IS}^{eff} will generally overestimate the true value.

Table 2 shows the obtained values of δ_{IS}^{eff} for T-MREV-*N*, $R18_2^5$ and REDOR experiments with the assumed rf inhomogeneity, for two-spin and three-spin simulations. The errors induced by rf inhomogeneity in the different experiments are in the range −2 to +4%. For the REDOR experiment, the errors induced by rf missetting (see also Fig. 7) are generally smaller than for the other pulse sequences. Accordingly, errors induced by rf-field inhomogeneity are relatively small, in the order of 1% or less in the assumed scenarios. The effects of remote ^{1}H spins and rf missettings partially compensate each other, as reported earlier [9].

3.7. Asymmetric dipolar couplings

So far, only axially symmetric dipolar-coupling tensors have been considered. Dipolar coupling tensors are indeed axially symmetric in the absence of molecular motion. In the case of non-axially-symmetric motion, dynamically-averaged dipolar-coupling tensors are, however, generally asymmetric, which has been observed previously in single-crystal samples of small molecules [63–65]. While the impact of non-axially-symmetric motion on deuterium quadrupolar line shapes is well documented [66] we are not aware of such observations in biomolecular MAS NMR. Fig. 12 investigates the sensitivity of the different recoupling sequences to such asymmetries. Shown are recoupling patterns using asymmetric dipolar coupling tensors and an asymmetry $\eta = (D_{yy} - D_{xx})/\delta_{IS}$ of 0, 0.3, and 0.6. In all sequences, asymmetry leads to a distinct change in the recoupling, as seen by a change in the dipolar line shape, which, in addition to well-defined 'horns' has some broader features (see frequency-domain data in Fig. S8 of the Supplementary Information). Equivalently, in time domain, the recoupling patterns appear dampened due to the asymmetry. In case of sufficient signal-to-noise, all sequences may allow to detect the line shape distortions (or, equivalently, the damping). However, in the case of T-MREV-*N*, the $R18_2^5$, and the CPPI sequences, the damping may also arise as a consequence of other coherent or incoherent (relaxation) mechanisms, and it may be very difficult to unambiguously identify the asymmetry. An exception in this respect is the REDOR experiment, where the normalization to reference experiments allows us to rule out relaxation as an explanation of the dampening. Therefore, the detection of asymmetric dipolar tensors by REDOR seems possible in particular in highly deuterated samples where the interaction with additional proton spins, the main source of systematic errors in REDOR experiments, is minimized.

We have shown above (Fig. 11) that extraneous proton spins have a noticeable effect on the REDOR recoupling. This apparent additional oscillation in REDOR recoupling might interfere with the ability to unambiguously identify the asymmetry of the dipolar-coupling tensor. To address this issue, we have investigated whether the coupling to an extraneous proton spin could be mistaken for an asymmetry of the N–H dipolar coupling of interest, i.e., whether a fitted dipolar asymmetry could be simply an artefact that originates from the influence of remote spins. We have, thus, fitted the REDOR recoupling curves of three-spin (H, H, N) systems against ideal two-spin H–N simulations, where the H–N coupling was allowed to be asymmetric. Fig. 13 shows that the apparent dipolar-coupling asymmetry η that results from the two-spin fit to the three-spin simulations is generally negligible in the situations considered. Dipolar-coupling asymmetries η above about 0.1 can, thus, be reliably extracted from REDOR data even in the

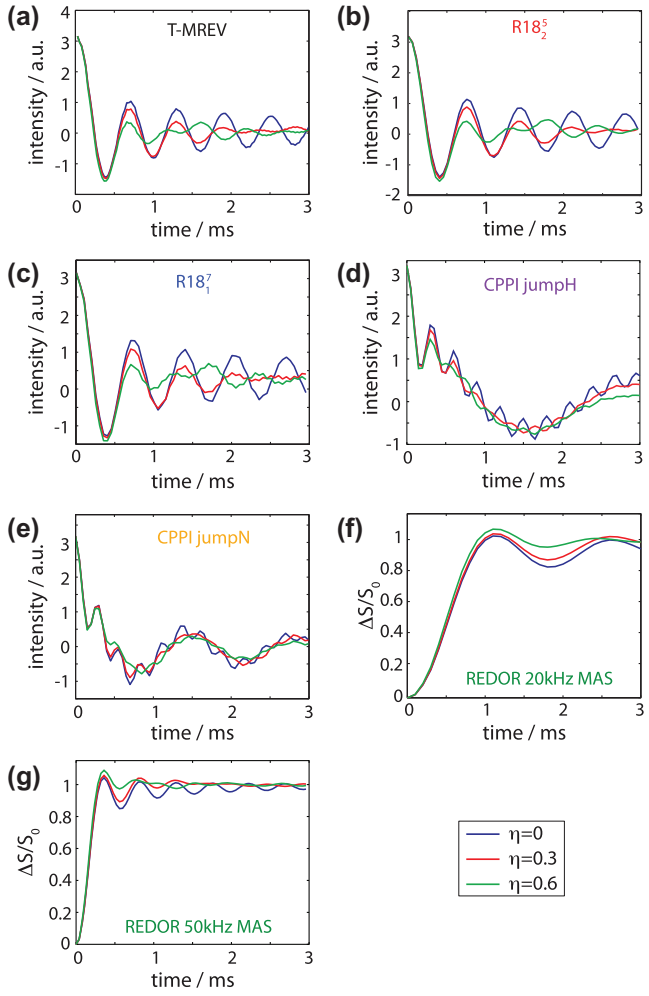

Fig. 12. Recoupling patterns for asymmetric dipolar couplings. Dipolar coupling asymmetries are $\eta = (D_{yy} - D_{xx})/\delta_{IS} = 0$ (blue), 0.3 (red), and 0.6 (green), keeping the anisotropy at 19.5 kHz (two-spin N–H system) and standard CSA tensor parameters. (For interpretation of the references to colour in this figure legend, the reader is referred to the web version of this article.)

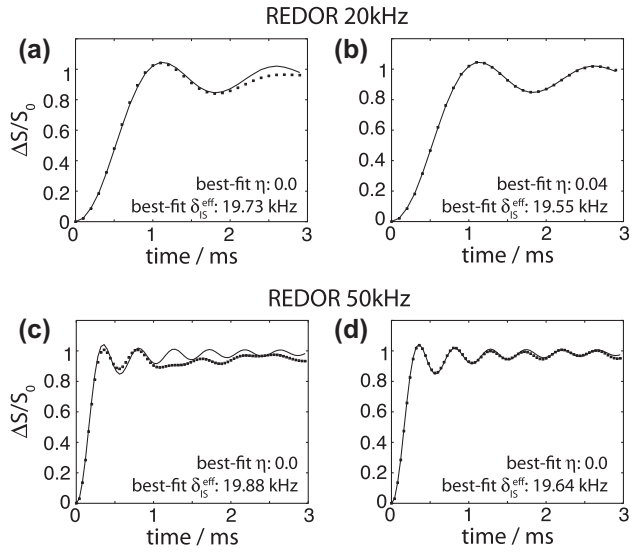

Fig. 13. Investigation of the effect of a remote proton spin on the fitted parameters of a general asymmetric dipolar coupling tensor. Data points show three-spin (N, H, H) simulations using the three-spin systems introduced in Fig. 11 with a ^{1}H–^{1}H coupling of 15 kHz (panels a and c) and 5.6 kHz (panels b and d), respectively. Solid lines show the best-fit two-spin simulations with asymmetric dipolar couplings (two fit parameters: δ_{IS}^{eff} and η). Panels a and b (c and d) assume 20 kHz (50 kHz) MAS frequency, and the timings as used before.

presence of residual protonation, as found in deuterated, back-exchanged protein samples.

We conclude from the discussion of the numerical simulations that the REDOR experiment is the most accurate experiment for the determination of one-bond dipolar couplings. It requires a high degree of deuteration in order to generate isolated ^{15}N–^{1}H spin pairs due to the sensitivity of the REDOR experiment to multiple couplings. Based on these results, we decided to experimentally characterize only the REDOR experiment in detail using a highly-deuterated sample, and proton-detected experiments. The above simulations show that the T-MREV experiment is also quite robust, and presents a good alternative. Because the proton-detected experiments performed on our sample require relatively fast MAS frequencies, which are incompatible with T-MREV, we did not experimentally investigate the T-MREV experiment.

4. Experimental data

For the measurements of N–H dipolar couplings, a crystalline sample of uniformly ^{2}H, ^{13}C, ^{15}N labeled ubiquitin was prepared as described earlier [9]. The protein was crystallized in a H_2O/D_2O mixture, resulting in incorporation of ^{1}H at about 30% of the exchangeable sites, i.e., amide sites as well as OH and NH side-chain sites [9]. All experiments were performed using a 1.8 mm triple-resonance probe (Ago Samoson, Tallinn) on a Bruker Avance 600 MHz spectrometer. The rotors were restricted to 40% of the length but the REDOR sequence also works with unrestricted samples. The pulse sequences are refocused-INEPT type HSQC [67] experiments, as shown in Fig. 1 and described elsewhere in more detail [9]. High-resolution proton detected ^{1}H–^{15}N spectra [68] can be obtained because of the strong isotopic dilution of ^{1}H spins at MAS frequencies above approximately 20 kHz.

We have recorded three different REDOR data sets, at 40 kHz MAS frequency. In data sets one and two, we have used ^{1}H π pulses with a nutation frequency of 125 kHz, and in data set three the pulses had an rf-field amplitude of 100 kHz. In all cases, the ^{15}N π pulse was applied at 50 kHz rf-field amplitude. The delay τ_s was set to 20.5 μs, 20 μs and 19.5 μs in data sets one, two and three, respectively. Pulse calibrations were obtained by varying the power level of the ^{1}H 90° pulse in a refocused INEPT element prior to the detection period in a HSQC-type experiment, fixing its duration to 4 μs and searching the zero crossing of the signal. Likewise, the ^{15}N 180° power level was found by fixing the length of the ^{15}N pulse that initiates the refocused INEPT block prior to detection to 10 μs, and varying its power level. Because isolated pulses are applied in REDOR, it seems advantageous to calibrate the pulses in a similar manner. Reference spectra were obtained by omitting the ^{1}H pulses, as described [9].

Fig. 14a–d shows representative examples of obtained recoupling curves. In a recent study, we have performed a joint analysis of these data, i.e., a common dipolar-coupling anisotropy was fitted simultaneously to the three recoupling curves. Here, we opted to perform a slightly different analysis, by fitting a general asymmetric dipolar-coupling tensor to each individual data set (solid lines). This fitting was done in a grid-search type manner, comparing numerical two-spin simulations to the experimental data. We used a 25 Hz grid step along the dimension of δ_{IS}^{eff} and a step size of 0.02 along η. The best-fit dipolar-coupling tensor parameters were obtained from the minimum of the reduced χ^2, defined as discussed previously [9]. Error bars were obtained from an inspection of the profile of the reduced χ^2, and are reported as the values of the anisotropy and asymmetry where the reduced χ^2 exceeds its

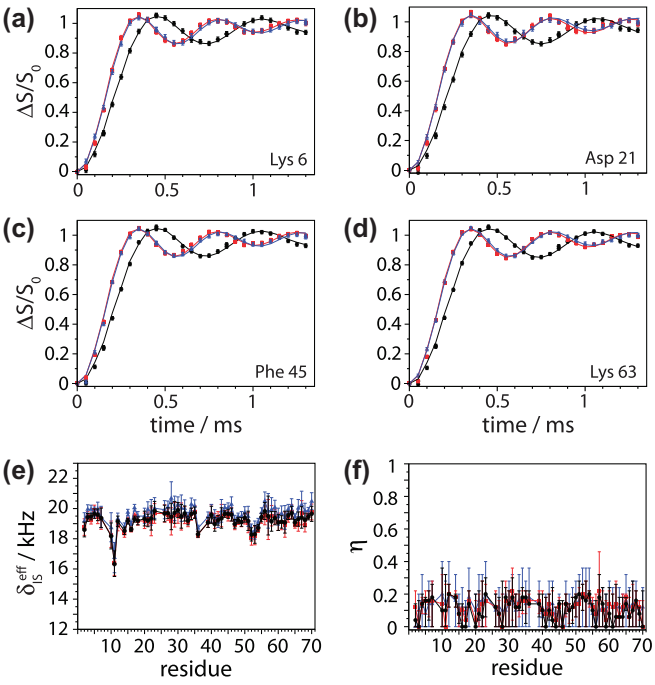

Fig. 14. Experimental REDOR data, measured on highly deuterated, 30% back-exchanged microcrystalline ubiquitin. Data shown in black, red and blue correspond to the three data sets, using different ^{1}H pulse widths and timing (black: 4 μs ^{1}H π pulse, τ_s = 20.5 μs; red: 4 μs ^{1}H π pulse, τ_s = 20 μs; blue: 5 μs ^{1}H π pulse, τ_s = 19.5 μs). (a)–(d) show representative recoupling curves, (e) and (f) show the best-fit δ_{IS}^{eff} and η, respectively, in a general two-parameter fit, as described in the text. (For interpretation of the references to colour in this figure legend, the reader is referred to the web version of this article.)

minimum by one. This assumes that the two parameters are uncorrelated, which we find to be fulfilled to a good approximation.

Fig. 14e and f show the best-fit values of the anisotropy and asymmetry, extracted from the three data sets. Within error margins, the three data sets agree with each other. Dipolar coupling anisotropies are essentially identical to values found from the joint analysis of the three data sets [9]. Reduced dipolar coupling anisotropy is found in loop regions as discussed previously. The asymmetry of the dipolar coupling is small. Indeed, there is no residue where the asymmetry differs significantly from zero in all three data sets, indicating that within the experimental precision we do not find evidence of anisotropic motion.

Our data, thus, demonstrate experimentally the possibility to obtain dipolar coupling parameters from the REDOR experiments, and show the principle of scaling the recoupling oscillation frequency by appropriate choice of the experimental parameters. We find here that the backbone motion is well-described by an isotropic model.

5. Conclusions and outlook

Using numerical simulations it was shown that the shifted finite-pulse REDOR experiment is clearly the best experiment among the tested sequences since it can be implemented over a large range of MAS frequencies and has the lowest systematic errors leading to the most accurate dipolar-coupling constants. Additional benefits of the REDOR experiment are the simple data fitting with only a single parameter and the possibility to measure asymmetric dipolar couplings due to anisotropic motional averaging. A challenge for the REDOR experiment is the sensitivity to the presence of multiple couplings, which comes from the absence of dipolar truncation in this experiment. Dilution of the proton network by deuteration is the most straightforward method to circumvent related artefacts. Of interest for studies of protein dynamics is the backbone amide N–H coupling. In a perdeuterated protein, with protons only on the exchangeable sites (amides), the largest couplings to additional protons lead generally only to small errors (<2%). Even further improvements in the accuracy can be obtained by further decreasing the proton density, as we have used in our sample, or by including remote proton spins in the numerical simulations, which, however, requires knowledge of the structure. For applications to C–H moieties in proteins, selective or sparse random protonation in an otherwise deuterated environment [16] is a viable route.

As an alternative at slower MAS frequencies, the T-MREV sequences give also quite accurate dipolar-coupling measurements even in systems with higher proton densities due to the partial averaging of homonuclear dipolar couplings. Data evaluation is more complicated than for the REDOR experiment since additional parameters like a phenomenological relaxation term or a zero-frequency offset are needed. We expect that the measurement of hetero- and homonuclear couplings in proteins will provide further insight into structural plasticity of proteins, and believe that this article provides a useful guideline for the choice and practical implementation of these experiments.

Acknowledgments

This work was supported by the Swiss National Science Foundation (Grant 200020_124611) and the ETH. P.S. acknowledges a post-doctoral fellowship from the ETH. We thank Bernd Reif and Veniamin Chevelkov for stimulating discussions and for sharing results from numerical simulations with us. René Verel and Thomas Westfeld are acknowledged for numerous scientific discussions and for help with the setup of experiments.

Appendix A. Supplementary data

Supplementary data associated with this article can be found, in the online version, at doi:10.1016/j.jmr.2011.03.015.

References

[1] W. Franks, D. Zhou, B. Wylie, B. Money, D. Graesser, H. Frericks, G. Sahota, C. Rienstra, J. Am. Chem. Soc. 127 (2005) 12291–12305.
[2] J.L. Lorieau, A.E. McDermott, J. Am. Chem. Soc. 128 (2006) 11505–11512.
[3] J. Lorieau, A. McDermott, Magn. Reson. Chem. 44 (2006) 334–347.
[4] J.L. Lorieau, L.A. Day, A.E. McDermott, Proc. Natl. Acad. Sci. 105 (2008) 10366–10371.
[5] V. Chevelkov, U. Fink, B. Reif, J. Am. Chem. Soc. 131 (2009) 14018–14022.
[6] J. Yang, M.L. Tasayco, T. Polenova, J. Am. Chem. Soc. 131 (2009) 13690–13702.
[7] J.J. Helmus, K. Surewicz, W.K. Surewicz, C.P. Jaroniec, J. Am. Chem. Soc. 132 (2010) 2393–2403.
[8] R. Schneider, K. Seidel, M. Etzkorn, A. Lange, S. Becker, M. Baldus, J. Am. Chem. Soc. 132 (2010) 223–233.
[9] P. Schanda, B.H. Meier, M. Ernst, J. Am. Chem. Soc. 132 (2010) 15957–15967.
[10] V. Chevelkov, U. Fink, B. Reif, J. Biomol. NMR 45 (2009) 197–206.
[11] N. Giraud, M. Blackledge, M. Goldman, A. Böckmann, A. Lesage, F. Penin, L. Emsley, J. Am. Chem. Soc. 127 (2005) 18190–18201.
[12] G.A. Morris, R. Freeman, J. Am. Chem. Soc. 101 (1979) 760.
[13] D.P. Burum, R.R. Ernst, J. Magn. Reson. 39 (1980) 163–168.
[14] K.H. Gardner, L.E. Kay, J. Am. Chem. Soc. 119 (1997) 7599–7600.
[15] N.K. Goto, K.H. Gardner, G.A. Mueller, R.C. Willis, L.E. Kay, J. Biomol. NMR 13 (1999) 369–374.
[16] S. Asami, P. Schmieder, B. Reif, J. Am. Chem. Soc. 132 (2010) 15133–15135.
[17] A. Pines, M.G. Gibby, J.S. Waugh, J. Chem. Phys. 59 (1973) 569.
[18] B. van Rossum, C. de Groot, V. Ladizhansky, S. Vega, H. de Groot, J. Am. Chem. Soc. 122 (2000) 3465–3472.
[19] V. Ladizhansky, S. Vega, J. Chem. Phys. 112 (2000) 7158–7168.
[20] M. Lee, W.I. Goldburg, Phys. Rev. 140 (1965) A1261–A1271.
[21] A. Bielecki, A.C. Kolbert, M.H. Levitt, Chem. Phys. Lett. 155 (1989) 341.
[22] A. Bielecki, A.C. Kolbert, H.J.M. de Groot, R.G. Griffin, M.H. Levitt, Frequency-switched Lee–Goldburg sequences in solids, in: W.S. Warren (Ed.), Advances in Magnetic Resonance, vol. 14, Academic Press, New York, 1990, pp. 111–124.

[23] S.V. Dvinskikh, H. Zimmermann, A. Maliniak, D. Sandstrom, J. Chem. Phys. 122 (2005) 044512.
[24] M. Hohwy, C.P. Jaroniec, B. Reif, C.M. Rienstra, R.G. Griffin, J. Am. Chem. Soc. 122 (2000) 3218–3219.
[25] M.H. Levitt, Symmetry-based pulse sequences in magic-angle spinning solid-state NMR, Encyclopedia of NMR, vol. 9, John Wiley & Sons Ltd., Chichester, 2002, pp. 165–195.
[26] X. Zhao, M. Eden, M.H. Levitt, Chem. Phys. Lett. 342 (2001) 353–361.
[27] X. Zhao, J.L. Sudmeier, W.W. Bachovchin, M.H. Levitt, J. Am. Chem. Soc. 123 (2001) 11097–11098.
[28] S.V. Dvinskikh, H. Zimmermann, A. Maliniak, D. Sandstrom, J. Magn. Reson. 164 (2003) 165–170.
[29] T. Gullion, J. Schaefer, J. Chem. Phys. 91 (1989) 7307.
[30] T. Gullion, J. Schaefer, Detection of weak heteronuclear dipolar coupling by rotational-echo double-resonance nuclear magnetic resonance, in: W.S. Warren (Ed.), Advances in Magnetic Resonance, vol. 13, Academic Press, New York, 1989, pp. 57–83.
[31] C.P. Jaroniec, B.A. Tounge, C.M. Rienstra, J. Herzfeld, R.G. Griffin, J. Magn. Reson. 146 (2000) 132–139.
[32] A.W. Hing, S. Vega, J. Schaefer, J. Magn. Reson. 96 (1992) 205.
[33] M. Hohwy, C.M. Rienstra, C.P. Jaroniec, R.G. Griffin, J. Chem. Phys. 110 (1999) 7983–7992.
[34] M. Baldus, Prog. Nucl. Magn. Reson. Spectrosc. 41 (2002) 1–47.
[35] D.M. Brink, G.R. Satchler, Angular Momentum, third ed., Clarendon Press, 1993.
[36] U. Haeberlen, J.S. Waugh, Phys. Rev. 175 (1968) 453.
[37] U. Haeberlen, High Resolution NMR in Solids: Selective Averaging, Academic Press, New York, 1976.
[38] M. Leskes, P.K. Madhu, S. Vega, Prog. Nucl. Magn. Reson. Spectrosc. 57 (2010) 345–380.
[39] M. Hohwy, N.C. Nielsen, J. Chem. Phys. 106 (1997) 7571–7586.
[40] T. Gullion, D.B. Baker, M.S. Conradi, J. Magn. Reson. 89 (1990) 479–484.
[41] M. Hohwy, C.M. Rienstra, R.G. Griffin, J. Chem. Phys. 117 (2002) 4973–4987.
[42] A. Grommek, B.H. Meier, M. Ernst, Chem. Phys. Lett. 427 (2006) 404–409.
[43] M.J. Bayro, M. Huber, R. Ramachandran, T.C. Davenport, B.H. Meier, M. Ernst, R.G. Griffin, J. Chem. Phys. 130 (2009) 114506.
[44] I. Scholz, J.D. van Beek, M. Ernst, Solid State Nucl. Magn. Reson. 37 (2010) 39–59.
[45] M. Ernst, H. Geen, B.H. Meier, Solid State Nucl. Magn. Reson. 29 (2006) 2–21.
[46] T.G. Oas, R.G. Griffin, M.H. Levitt, J. Chem. Phys. 89 (1988) 692.
[47] M.H. Levitt, T.G. Oas, R.G. Griffin, Isr. J. Chem. 28 (1988) 271–282.
[48] M. Eden, M.H. Levitt, J. Chem. Phys. 111 (1999) 1511–1519.
[49] A. Brinkmann, M. Eden, M.H. Levitt, J. Chem. Phys. 112 (2000) 8539–8554.
[50] M. Carravetta, M. Eden, X. Zhao, A. Brinkmann, M.H. Levitt, Chem. Phys. Lett. 321 (2000) 205–215.
[51] E. Vinogradov, P. Madhu, S. Vega, Strategies for high-resolution proton spectroscopy in solid-state nmr, in: New Techniques in Solid-State NMR, Topics in Current Chemistry, vol. 246, 2004, pp. 33–90.
[52] F. Dyson, Phys. Rev. 75 (1949) 486.
[53] C.M. Rienstra, M. Hohwy, L.J. Mueller, C.P. Jaroniec, B. Reif, R.G. Griffin, J. Am. Chem. Soc. 124 (2002) 11908–11922.
[54] W.K. Rhim, D.D. Elleman, R.W. Vaughan, J. Chem. Phys. 59 (1973) 3740.
[55] P. Mansfield, M. Orchard, D. Stalker, K. Richards, Phys. Rev. B 7 (1973) 90–105.
[56] S. Smith, T. Levante, B.H. Meier, R.R. Ernst, J. Magn. Reson., Ser. A 106 (1994) 75–105.
[57] H.H. Suzukawa, V.B. Cheng, M. Wolfsberg, J. Chem. Phys. 59 (1973) 3992.
[58] J.C.C. Chan, R. Tycko, J. Chem. Phys. 118 (2003) 8378–8389.
[59] B. Wylie, W. Franks, C. Rienstra, J. Phys. Chem. B 110 (2006) 10926–10936.
[60] K. Loth, P. Pelupessy, G. Bodenhausen, J. Am. Chem. Soc. 127 (2005) 6062–6068.
[61] E. Chekmenev, Q. Zhang, K. Waddell, M. Mashuta, R. Wittebort, J. Am. Chem. Soc. 126 (2004) 379–384.
[62] J. Hall, D. Fushman, J. Am. Chem. Soc. 128 (2006) 7855–7870.
[63] B.H. Meier, F. Graf, R.R. Ernst, J. Chem. Phys. 76 (1982) 767.
[64] J. Tritt-Goc, N. Pilewski, U. Haeberlen, Chem. Phys. 102 (1986) 133–140.
[65] J. Tritt-Goc, J. Phys. Chem. Solids 56 (1995) 935–942.
[66] H. Spiess, Adv. Polym. Sci. 66 (1985) 23–58.
[67] G. Bodenhausen, D.J. Ruben, Chem. Phys. Lett. 69 (1980) 185–189.
[68] V. Chevelkov, K. Rehbein, A. Diehl, B. Reif, Angew. Chem., Int. Ed. 45 (2006) 3878–3881.